buildings

MDPI

Article

Bidirectional Scattering Distribution Function (BSDF) Resolutions for Solar Shading Devices

Mandana Sarey Khanie [1,*], Mikkel Kofod Pedersen [2,*], Frederik Rasmussen [3], Edward Michael Barrett [1] and David Geisler-Moroder [4,*]

[1] Institute for Environmental Design and Engineering (IEDE), The Bartlett Faculty of the Built Environment, University College London, London WC1H 0NN, UK; edward.barrett@ucl.ac.uk
[2] Ladybug Tools LLC, 2993 Eskridge Road, Fairfax, VA 22031-2269, USA
[3] Danish Technological Institute, Gregersensvej 8, 2630 Høje Taastrup, Denmark; fras@teknologisk.dk
[4] Unit of Energy Efficient Building, University of Innsbruck, Technikerstraße 13, 5th floor south wing, 6020 Innsbruck, Austria
* Correspondence: m.khanie@ucl.ac.uk (M.S.K.); mikkel@ladybug.tools (M.K.P.); david.geisler-moroder@uibk.ac.at (D.G.-M.)

Abstract

This paper investigates the influence of bidirectional scattering distribution function (BSDF) resolution on daylight simulations. Seven representative shading systems were selected and evaluated using a single-office model defined according to established recommendations. The tool *genBSDF* was used to generate BSDFs at different resolutions. Both annual climate-based and point-in-time daylight simulations were performed. The results show that BSDF resolution has only a minor impact on annual daylight metrics when compared with TT6, used here as the highest-resolution numerical reference, with maximum NRMSE values relative to TT6 of 0.04 for DA_{300}, 0.01 for cDA_{300}, and 0.02 for $UDI_{100–3000}$ across the investigated systems. Lower-resolution BSDFs (e.g., TT3, TT4, or Klems) are therefore adequate for annual illuminance-based assessments under the conditions studied. In contrast, point-in-time simulations were substantially more sensitive to resolution when direct sunlight penetrated the shading system; for example, NRMSE for one investigated system decreased from 0.63 with TT3 and 0.25 with TT4 to 0.11 with TT5. Lower resolutions also showed greater deviations in the spatial distribution of illuminance, particularly at the transition between directly sunlit and shaded regions. TT5 generally showed close agreement with TT6 while requiring substantially less BSDF-generation time. The findings therefore support selecting BSDF resolution according to simulation purpose: lower resolutions can be used efficiently for annual daylight metrics, whereas higher resolutions, such as TT5 or TT6, are recommended for detailed point-in-time assessments involving strong directional or direct-solar transmission. These findings therefore describe the sensitivity of daylight simulation outcomes to BSDF resolution and their convergence towards TT6, used as the highest-resolution numerical reference, rather than the absolute accuracy of the simulations.

Keywords: BSDF resolution; solar shading; complex fenestration systems; Klems; tensor tree

Check for updates

Academic Editor: Francesco Nocera

Received: 2 September 2026
Revised: 4 October 2026
Accepted: 16 October 2026
Published: 2 November 2026

Copyright: © 2026 by the authors. Licensee MDPI, Basel, Switzerland. This article is an open access article distributed under the terms and conditions of the Creative Commons Attribution (CC BY) license.

1. Introduction

The buildings and construction sector accounts for approximately 34% of global energy consumption and contributes up to 37% of energy- and process-related CO_2 emissions [1]. Within this sector, lighting represents a significant portion of electricity usage.

In 2019, building electricity consumption constituted more than 18% of the global electricity demand [2].

Maximising daylight access is an important strategy for reducing reliance on artificial lighting and energy consumption, while also supporting occupant well-being, comfort, productivity, and satisfaction with the indoor environment [3]. However, increased daylight penetration can also lead to higher cooling demands due to excessive solar heat gains, particularly during warmer periods. To mitigate these effects while maintaining visual comfort and daylight availability, complex fenestration systems (CFS) can be used. These combine light-transmitting window technologies with integrated non-transparent layers or layers featuring switching properties [4]. Such systems can enhance thermal and visual comfort, but can also influence users' connection to the outdoor environment [5,6] and introduce design challenges by altering the appearance of colours, dimensions, or surface properties [7]. Therefore, while CFS offer multiple benefits, selecting an appropriate system remains a challenge. Reliable and computationally efficient simulation methods are therefore important for evaluating their daylight performance. More broadly, reliable daylight simulation also contributes to integrated building-performance assessment, where daylight and visual comfort are considered alongside energy performance, thermal conditions, and other aspects of indoor environmental quality.

CFS modelling methods are becoming increasingly important in characterising the directional transfer of solar and daylight flux in window systems [8]. Radiance [9] is a lighting simulation engine that predicts illumination levels using physically based ray tracing [10]. However, representative input data on geometry, materials, and weather conditions are required to obtain reliable daylight predictions. Increasing the resolution of input data can provide a more detailed representation of the physical system, but generally increases data-generation and computational requirements. Understanding how input resolution affects simulation results is therefore important for selecting an appropriate balance between computational demand and the level of detail required for a given application. One of the latest adoptions is the use of high-resolution variable bidirectional scattering distribution functions (BSDFs). BSDFs are mathematical functions [11] acting as a proxy for the geometry and describing flux transfer of light through a CFS [12]. Figure 1 illustrates the connection between the physical and mathematical representation of the electromagnetic waves that encounter a CFS. The mathematical expression of a BSDF describes the scattered (outgoing) radiance in direction (θ_2, φ_2) as a function of incident irradiance from direction (θ_1, φ_1).

$$\mathrm{BSDF}(\omega_1, \omega_2) = \frac{\mathrm{d}L_2(\omega_2)}{\mathrm{d}E_1(\omega_1)} \tag{1}$$

where:

ω_1, ω_2 are denote the incident and outgoing directions, respectively, each defined by its polar and azimuthal angles (θ_1, φ_1) and (θ_2, φ_2), respectively

E_1 is the incoming irradiance

L_2 is the outgoing radiance

While analytical BSDF models are generally used in computer graphics, BSDF data for CFS are usually provided in tabulated form, i.e., as a discrete set of values for a defined number and set of incident and outgoing directions. BSDF resolution refers to the level of detail at which the bidirectional scattering distribution function is tabulated, that is, the number of discrete directions. It defines how finely the incident and exiting hemispheres are divided into discrete patches for simulation and measurement purposes [12,13]. Various types of angular bases have been introduced for various purposes. The most commonly applied angular basis is full Klems [14] based on a BSDF resolution of 145 patches, both

for incoming and outgoing directions, which yields a 145 × 145 matrix or 21,025 data values. The patches have roughly the same projected solid angle. The numbering of the ingoing and outgoing hemispheres makes use of a coordinate axis reversal, meaning that the starting number (except 1) of each band in the outgoing hemisphere is placed at 180° along azimuth relative to the starting number of the incident hemisphere. Table 1 provides an overview of the number of patches (ϕ) within each band.

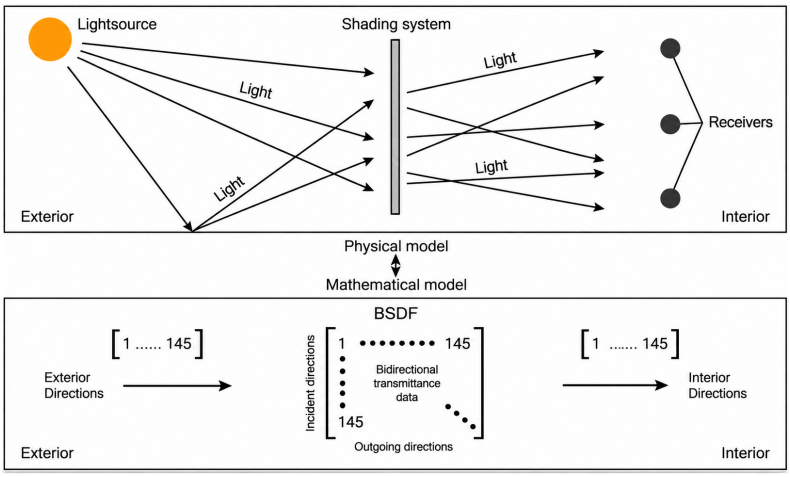


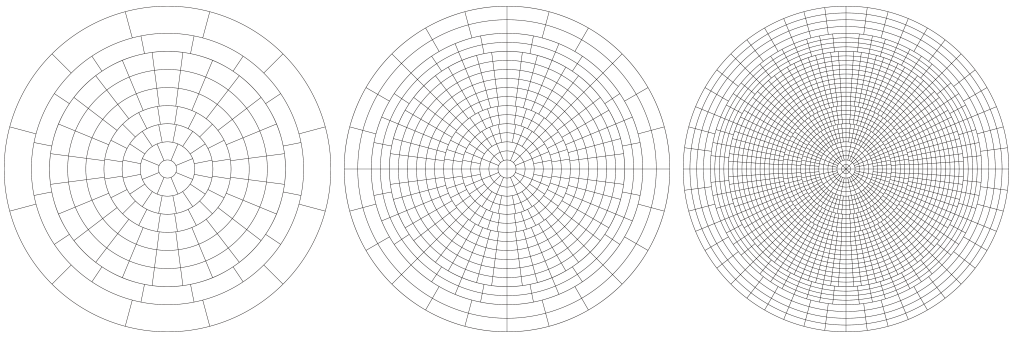
Figure 1. Schematic illustration of the physical light-transfer process through a CFS and its discretised BSDF representation, shown here using the full Klems basis as an example. Light from a source is transmitted through a CFS and ultimately reaches interior receivers. This physical process is mathematically modelled using a BSDF represented by a 145 × 145 matrix (full Klems discretisation). The incoming light is discretised into 145 patches, each representing a different incident direction. Similarly, the outgoing light is discretised into 145 interior patches (solid angles), each representing a different outgoing direction. The BSDF matrix describes how light is scattered from each incoming direction (exterior) to each outgoing direction (interior) using non-negative coefficients ($c \geq 0$). These coefficients are arranged in a 145 × 145 table. Each column represents a distinct incoming direction, and each row a distinct outgoing direction. Each cell in the table holds the coefficient that determines how much light is scattered from the corresponding incoming direction to the corresponding outgoing direction.

Table 1. Overview of the full Klems subdivision of the hemisphere including angular range and number of patches in each band.

Band	θ-Range	Average θ	Number of ϕ
1	0–5	0	1
2	5–15	10	8
3	15–25	20	16
4	25–35	30	20
5	35–45	40	24
6	45–55	50	24
7	55–65	60	24
8	65–75	70	16
9	75–90	82.5	12

Each column in the matrix represents a single incidence patch. Each column of the BSDF matrix represents an incident direction and contains 145 coefficients describing the scattering distribution across the outgoing directions. The contribution to transmitted flux depends on the BSDF coefficients and the corresponding angular weighting. The rows of the matrix thus hold data of the outgoing scattering. Due to the axis reversal, a purely specular system will give a diagonal matrix for both the transmission and reflection. The half Klems

and quarter Klems bases have lower resolutions than the full Klems basis. The half Klems has a 73 × 73 grid (5329 values), while the quarter Klems uses a 41 × 41 grid (1681 values). Both maintain the same numbering system as the full Klems basis. To increase angular resolution, the angle basis can be further subdivided. Based on the full Klems grid, each patch can be split **n** times. Common discretizations of the angle bases found in literature is either the 2× Klems and 4× Klems as seen in Figure 2. As the resolution increases, so does the data size. In 4× Klems, many values may not be equally significant. To optimise this, a variable-resolution tensor tree can be used, assigning finer detail only to areas with high-intensity variations.



(**a**) (**b**) (**c**)

Figure 2. Discretisation of the Klems angle basis: (**a**) 1× Klems; (**b**) 2× Klems; (**c**) 4× Klems.

Among other existing angle bases [15,16], Shirley-Chiu tensor tree basis BSDFs [17] use variable resolution, which allows for higher resolution where the distribution is non-uniform or has peaks. The tensor tree BSDFs will thus only have a higher resolution where it matters, while the resolution remains lower where the distribution is smooth. This is highly beneficial since it allows high-resolution BSDFs to be represented more efficiently than the high-resolution discretisation of the subdivided Klems angle basis. In two sets of reports from the IEA SHC Task 61 [12,13], the BSDF generation and analysis are reported in detail, which in the meantime has led to the preparation and initiation of a standardisation project [18] for BSDF data generation.

Geisler-Moroder et al. [19] provide a comprehensive overview of studies performed to validate the workflow of BSDF data generation and usage in CBDM simulations. This also includes key research on usage of high-resolution and low-resolution BSDF data. In 2011, Ward et al. [20] analysed the effect of discretisation schemes for both the sky dome and the BSDF data. There, they indicated that a variable resolution would allow efficient representation of peaky distributions. McNeil and Lee [21] validated the Radiance Three-Phase method for annual daylight simulations, showing that low-resolution Klems BSDFs are appropriate for annual workplane illuminance results. Lee et al. [22] emphasized the use of variable resolution tensor tree BSDFs with high basis resolution (4096 × 4096) for simulating daylight redirecting systems and venetian blinds. They showed that the Five-Phase method, using high-resolution BSDF data for the direct solar component, outperforms the Three-Phase method also for illuminance-based calculations. Grobe [23] highlighted the importance of high-resolution BSDF Data for evaluating luminance-based metrics, e.g., for visual comfort assessments. To overcome limitations in terms of computational demand, they proposed using photon mapping instead of classic backward raytracing to sample these high-resolution BSDFs. Ward et al. [24] showed that the BSDF resolution significantly impacts the accuracy of daylight simulations, particularly for systems with a direct solar component. These contributions cannot always be represented adequately even with high-resolution BSDFs using 4096 × 4096 or 16,384 × 16,384 discretisations, which

are practical limits due to computational constraints. Therefore, they introduced a peak extraction algorithm that allows isolating the direct solar component from the BSDF data.

A preliminary study of a limited set of systems provided evidence that low-resolution BSDFs can be used for evaluations based on integral metrics (illuminance- or irradiance-based) [25]. Previous studies generally indicate that increasing BSDF resolution can improve the representation of directional light transmission. However, the extent to which increasing BSDF resolution influences daylight simulation results, and the resolution required relative to the associated computational demand, remain unclear.

The present study builds on previous findings by quantitatively evaluating the influence of BSDF resolution on daylight simulation results for seven representative shading systems. Both annual climate-based daylight metrics and point-in-time illuminance distributions are examined. Using TT6 as the highest-resolution numerical reference, the study investigates how deviations vary with BSDF resolution, shading-system characteristics and spatial position within the room. The results provide further evidence for assessing whether lower-resolution BSDFs are sufficient for annual daylight calculations, as proposed in the IEA SHC Task 61 white paper [12], and identify conditions where higher resolution is required.

Shading Systems

A wide variety of shading devices is available, including fixed and dynamic systems and external, internal, and between-glazing solutions [7], influencing their selection and performance. Additionally, shading systems can be distinguished by their ability to manage both diffuse radiation and direct sunlight [26]. One common classification considers their angular selectivity—the ability to block direct solar radiation while allowing diffuse light into the occupied space [6]. Systems with a high degree of angular selectivity include louvers, blinds, and overhangs, whereas other shading devices exhibit reduced angular selectivity, so their performance remains largely independent of the sun's angle of incidence. Beyond their interaction with solar radiation, their effectiveness in filtering daylight and reducing solar gains also depends on geometry, texture, and application [27]. Given the wide range of available shading devices, the present study focuses on a subset of systems commonly used in practice. The final set of shading systems and slat configurations was selected based on commercially available systems in the Danish context in which the study was conducted. The resulting set included Venetian blinds, expanded-metal shading systems, and micro-structures integrated into glazing. Venetian blinds, commonly found in temperate climates, consist of adjustable slats available in different shapes and sizes, offering flexibility in controlling daylight and solar gains [7]. Their simplicity and cost-effectiveness contribute to their continued prevalence. Similarly, expanded metal mesh shading is increasingly incorporated into building facades, particularly in large office and industrial buildings, due to its affordability and ease of manufacturing. Venetian blinds are also frequently represented in simulation studies using BSDF data [8,28]. While shading geometry and configuration directly influence daylight distribution and performance [29,30], the present study does not investigate the optimisation of shading geometry itself. Instead, it focuses on how these systems are represented through BSDF data, and specifically on the resolution required to adequately represent their directional light-transmission characteristics in daylight simulations.

2. Methodology

This study presents a procedural framework for analysing the sensitivity of illuminance-based daylight metrics to BSDF resolution using seven shading-system variations. The selected daylight metrics were evaluated both on an annual basis and using point-in-time

simulations. The daylight simulation workflow was implemented within a Radiance-based Bash scripting environment, supporting automation and reproducibility. Simulations were performed using the matrix-based Five-Phase Method, which enables CFS to be modelled using high-resolution BSDF data. For the climate-based analysis, occupied hours were defined as 08:00–17:00. The simulation results were processed and visualised using Python (version 3.7.0) for subsequent analysis. Manual occupant operation of the shading systems was not included. Further details of the simulation parameters and procedures are provided in the following sections.

2.1. Case Study

The "shoebox" reference office defined in [31] was used as the basis for the case-study model. The office is a side-lit room with six workplaces, including a desk, a chair, and a PC. The interior dimensions are 3.6 m × 8.2 m × 2.8 m, resulting in 29.52 m^2 of office space. The window opening is located on one side of the office, with a sill height of 1 m, and measures 3 m × 1.5 m. The dimensions, window location, and floor are shown in Figure 3. The interior window-to-wall ratio (WWR) of the window opening is 45% while the exterior WWR is 39%. The frame and mullion of the window are 0.05 m wide, and the frame factor is therefore 16%. The resulting glazed area measures 2.9 m × 1.4 m, while there is 0.35 m to either side of the interior wall. The optical properties of the materials used in the "shoebox" are listed in Table 2. The glazing comprises clear glass with a visible transmission of τ_{vis} of 65%. This glazing was selected to minimise scattering effects from the glazing itself, thereby allowing the influence of the CFS to dominate the comparison. The reference office was south-facing, and Copenhagen weather data were used for the daylight simulations.

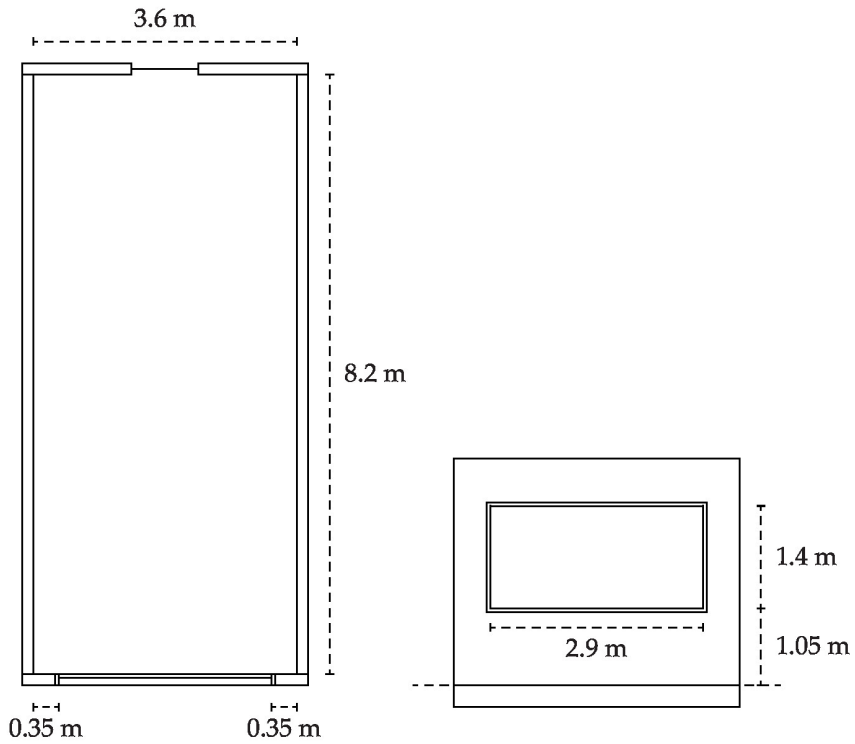


Figure 3. Dimensions of the reference office used in the simulations.

Table 2. Optical material properties from MIT's reference office [31].

Material	Properties
Interior Walls	Lambertian diffuser with a 50% reflectance
Exterior Walls	Lambertian diffuser with a 50%/35% (inside/outside) reflectance
Ceiling	Lambertian diffuser with a 80% reflectance
Floor	Lambertian diffuser with a 20% reflectance
External Ground	Lambertian diffuser with a 20% reflectance

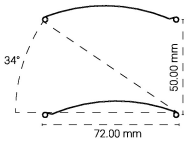
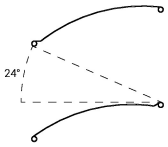
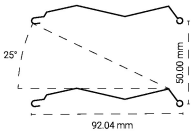
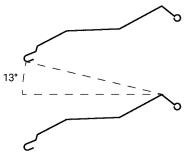
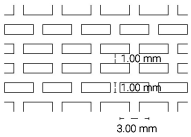
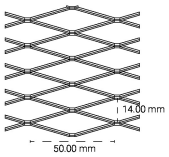
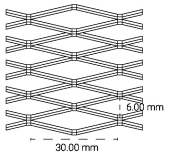
2.2. Selection of the Shading Systems

The seven shading-system variations shown in Table 3 represent four distinct shading systems, three of which include a second configuration differing in either slat rotation or opening size. The first shading system is a Venetian blind with curved slats. The distance from front to back is 72 mm, and the slat spacing is 50 mm. The first variant, Shade_1A, has a cut-off angle of 34°. In Shade_1B, the slats are rotated to produce a smaller cut-off angle of 24°. The shading system is inspired by the product Solomatic 4A by Blendex A/S, Gentofte, Denmark. The second shading system is a Venetian blind with a different slat geometry. The distance from front to back is 92 mm, and the slat spacing is 50 mm. The first variant, Shade_2A, has a cut-off angle of 25°. The second variant, Shade_2B, has its slats rotated, creating a smaller cut-off angle of 13°. The shading system is inspired by the product Lamisol 4B by Blendex A/S, Gentofte, Denmark. The third shading system is a perforated sheet with rectangular cut-outs. The length of the holes is 3 mm, and the height is 1 mm. The width of the solid parts is 1 mm. The fourth and final shading system is an expanded-metal panel with rhombic openings. The first variant, Shade_4A, has openings with a width of 50 mm, and a height of 14 mm. The second variant, Shade_4B, has openings with a width of 30 mm, and a height of 6 mm. All shading systems are modelled with a single glass pane placed 30 mm from the shading geometry. The Radiance glass material was defined using a transmissivity corresponding to a visible transmittance of 65%.

All shading systems have the same surface material. The shading-system variants were selected to enable controlled within-system comparisons. For Shade_1A/1B and Shade_2A/2B, the basic geometry and material properties were maintained while the slat rotation and corresponding cut-off angle were varied. For Shade_4A/4B, the same expanded-metal system and material were maintained while the opening dimensions were varied. Across all BSDF-resolution comparisons, the shading geometry, material properties, room model, orientation, climate and simulation parameters were kept unchanged, allowing the effect of BSDF resolution to be evaluated under otherwise consistent conditions. The surface material was defined according to the RAL colour-matching system. RAL 9006 (Weissaluminium), with a reflectance of 0.5363, was used for all shading systems. A specularity value of 0.065 was assigned to represent the glossy finish.

```
#Shading material                    #Glazing properties
void plastic blind                   void glass glazing
0                                    0
0                                    0
5 0.4394 0.5694 0.5907 0.065 0.0     4 0.708456 0.708456 0.7084569 1.52
```

Table 3. Overview of selected shading systems.

Shading System	Geometry	Material	Reflectance	Type	Company
1A		RAL 9006 weissaluminium	0.5363	Venetian blind	Blendex (Louisville, KY, USA)
1B		RAL 9006 weissaluminium	0.5363	Venetian blind	Blendex
2A		RAL 9006 weissaluminium	0.5363	Venetian blind	Blendex
2B		RAL 9006 weissaluminium	0.5363	Venetian blind	Blendex
3		RAL 9006 weissaluminium	0.5363	Perforated sheet	None
4A		RAL 9006 weissaluminium	0.5363	Expanded metal	None
4B		RAL 9006 weissaluminium	0.5363	Expanded metal	None

2.3. Simulation Framework

The matrix-based Five-Phase method framework consisted of several stages, including BSDF generation, model definition, analysis-grid generation, and parameter selection. The simulation parameters were defined through a convergence study. The illuminance calculation within the matrix-based Five-Phase Method [32] was implemented in three parts:

- Part 1: Three-Phase simulation
- Part 2: Direct solar part of the Three-Phase simulation
- Part 3: Direct Sun Coefficients Simulation

The simulation workflow was implemented using Radiance and compiled into a single Bash script containing the required command lines. Here, the same folder structure used by [32] is adopted to support the workflow.

For systems like those investigated here, where the geometry and material information are available, the system model could be used in Part 3 for the direct sun contributions. However, for many systems this information is not available. Our study aims to analyse the influence of BSDF data resolution in general. TT6 (4096 × 4096) was selected as

the highest resolution considered practically feasible in terms of BSDF generation, data size, and computational demand. It therefore serves as the highest-resolution numerical reference for the resolution-sensitivity analysis.

2.3.1. BSDF Generation

The open-source Radiance engine [9], along with its associated tools, was utilised for setting up and executing the entire daylight simulation workflow. BSDF datasets were generated using the Radiance *genBSDF* tool. Previous studies have shown that *genBSDF* [22] is suitable for generating BSDF data as a virtual goniophotometer [8,33,34]. The input geometry to *genBSDF* was created according to the LBNL WINDOW coordinate system, in which +Z points towards the room interior and +Y points upwards. The whole model of the shading system must be placed in the -Z half space. Geometry extending beyond $Z = 0$ may not be included correctly in the ray-tracing process The parameters used in the generation of the BSDF data are important to ensure symmetry in the scattering distribution since the shading systems are symmetrical. Too few sampling rays may inadequately represent the system because sampling noise increases as the number of rays decreases. All datasets are generated using the same parameters. The common parameters are: -c 4000 -r '-ab 7 -ad 5000'. Each shading system also required parameters defining the geometry sampling area through the -dim option. Setting the boundary dimensions (-dim) forces the sampling rays to originate within the boundaries to avoid rays at the edges of the geometry, which can lead to sampling rays exiting the shading system without any intersection with geometry. The bounding dimensions varied for the shading systems, but a common feature for all bounding dimensions is that they are placed at the center of the geometry. All BSDFs are generated using the Linux version of Radiance under Ubuntu Linux on a virtual machine. The processor of the host machine is Intel® Core™ i7-7700 CPU (Intel Corporation, Santa Clara, CA, USA) 3.60 GHz with four cores available. Unless modified, the standard settings for *genBSDF* generate the full Klems resolution. Discretisation of the Klems angle basis can be made, though it requires modification of the code in the programs. No parameters or input are needed to specify the use of full Klems resolution.

A tensor-tree BSDF is specified as a rank-3 or rank-4 tensor tree together with a value n defining its maximum resolution. The directional subdivision follows the formula $2^n \times 2^n$. Thus for $n = 6$ TT6, each hemisphere can be subdivided into a maximum of $64 \times 64 = 4096$ directional regions. These 4096 regions describe the directional resolution of each hemisphere; the complete BSDF relates up to 4096 incident regions to up to 4096 outgoing regions and is therefore referred to in this study as having a 4096×4096 incident-by-outgoing basis resolution. Increasing n by one doubles each subdivision dimension, so that $n = 7$ corresponds to $128 \times 128 = 16,384$ directional regions per hemisphere.

The BSDFs are visualised in BSDFViewer for one incidence angle. Figures 4–10 show the selected shading systems, their BSDFs, and a drawing of their geometry. The tensor-tree BSDFs are presented in increasing order of resolution to allow comparison. The yellow patch in the Klems incident hemisphere indicates the angular patch containing the selected incident direction, while the × symbol in the tensor-tree incident hemisphere marks the selected incident direction ($\theta = 16.16°$, $\varphi = 90°$).

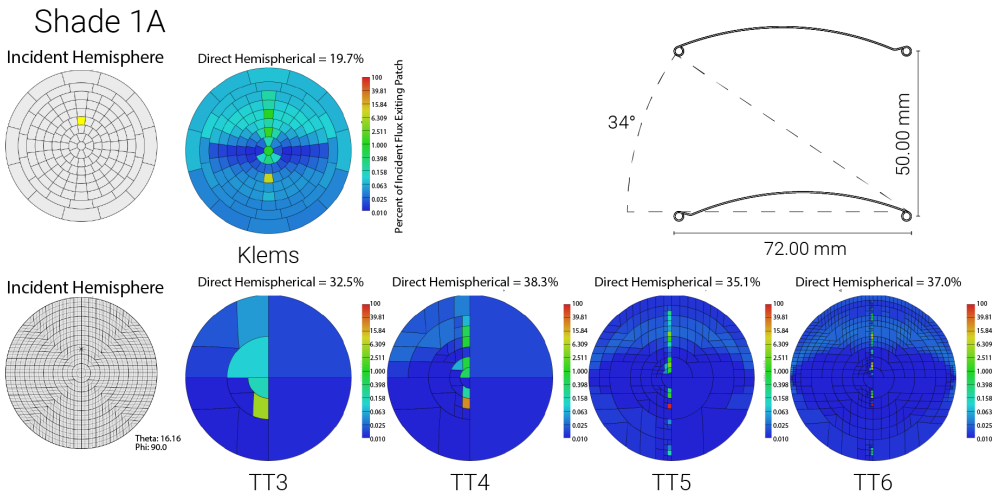


Figure 4. Overview of BSDFs of Shade 1A. The BSDFs are visualised for one incidence angle.

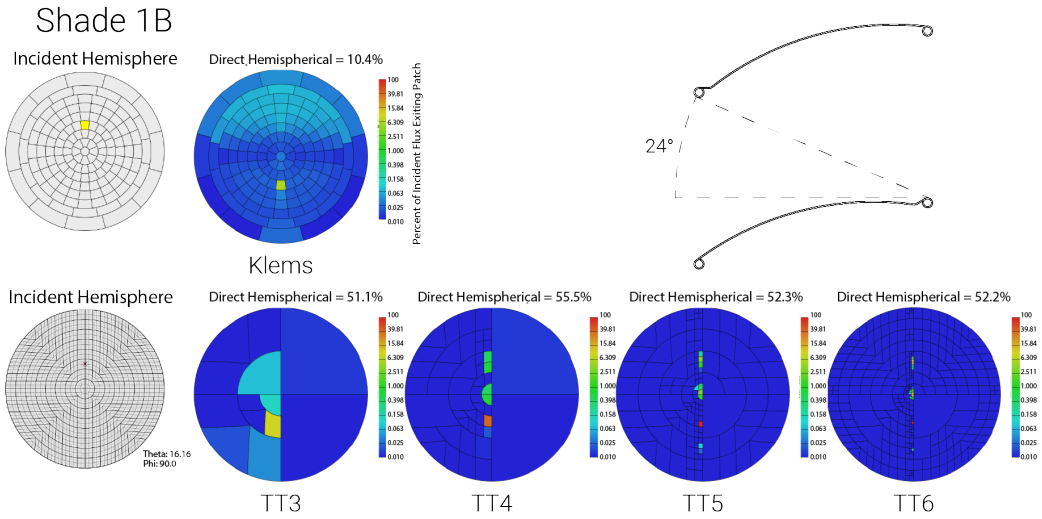


Figure 5. Overview of BSDFs of Shade 1B. The BSDFs are visualised for one incidence angle.

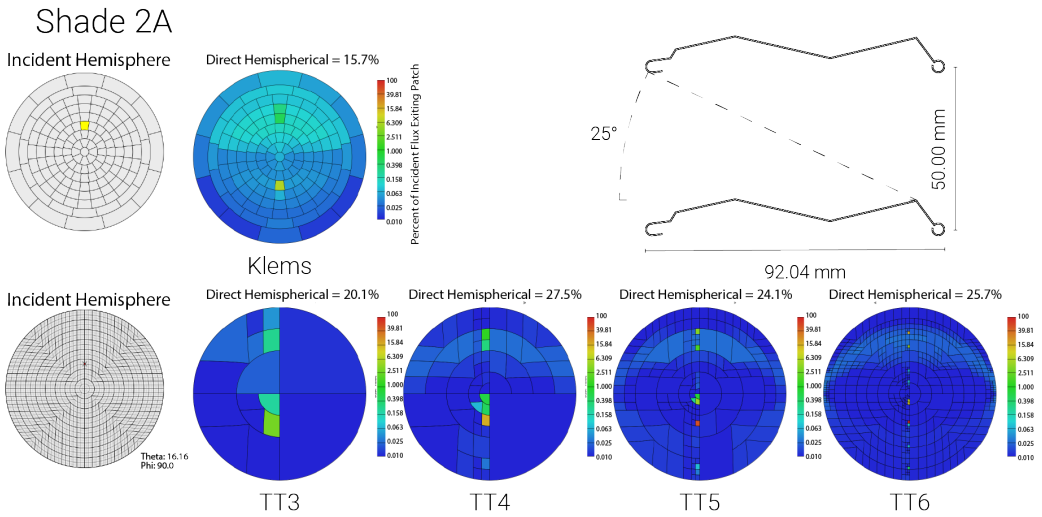


Figure 6. Overview of BSDFs of Shade 2A. The BSDFs are visualised for one incidence angle.

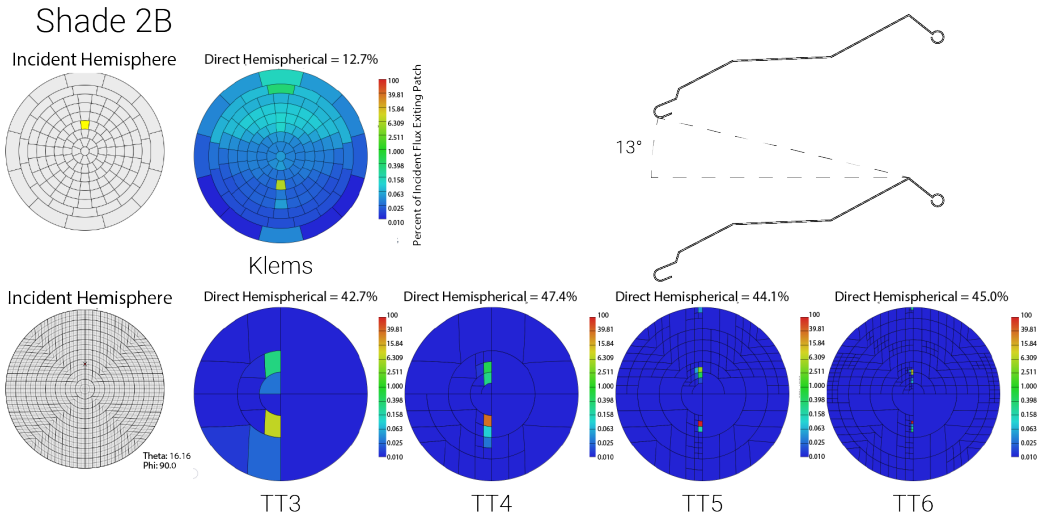


Figure 7. Overview of BSDFs of Shade 2B. The BSDFs are visualised for one incidence angle.

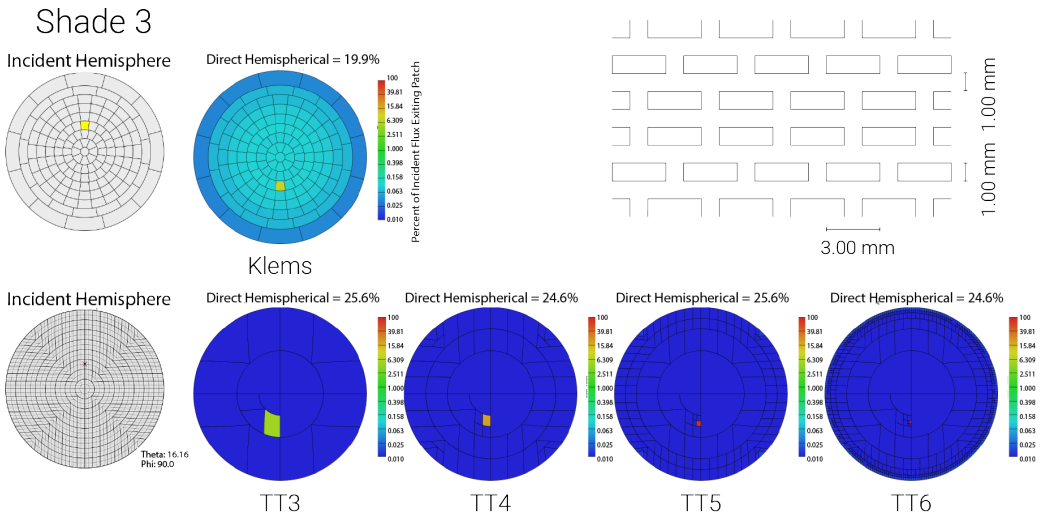


Figure 8. Overview of BSDFs of Shade 3. The BSDFs are visualised for one incidence angle.

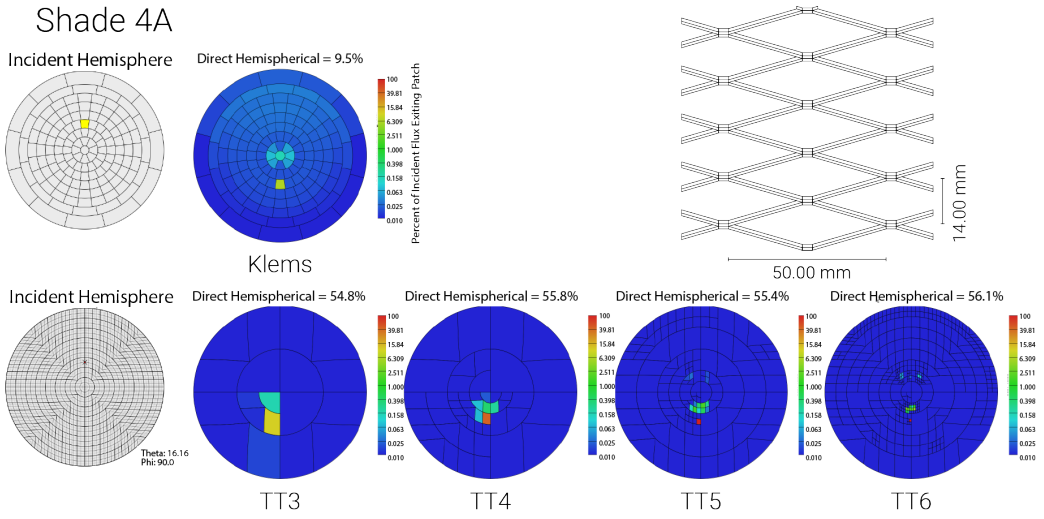


Figure 9. Overview of BSDFs of Shade 4A. The BSDFs are visualised for one incidence angle.

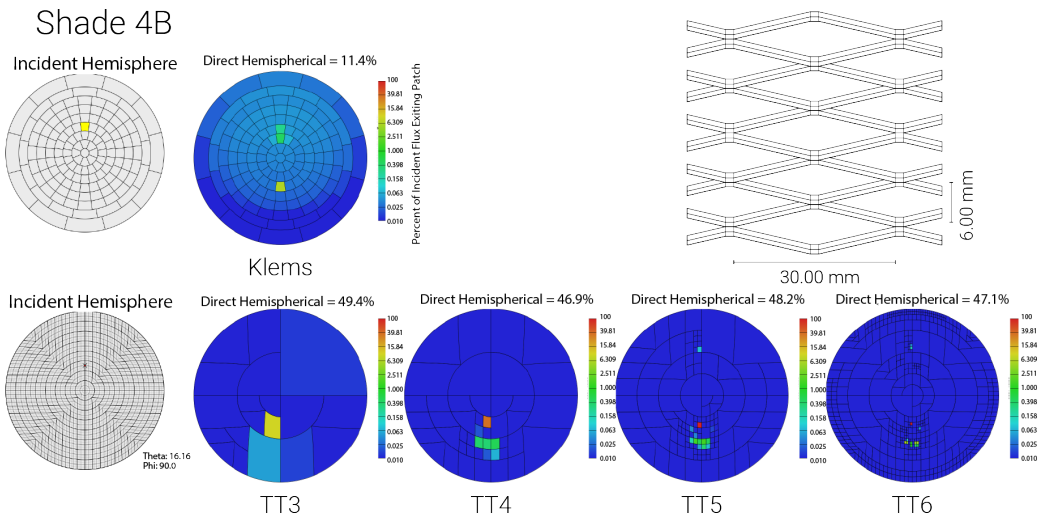


Figure 10. Overview of BSDFs of Shade 4B. The BSDFs are visualised for one incidence angle.

2.3.2. Analysis Grid

The analysis grid is based on the floor surface of the room. The boundaries are offset by 0.5 m, creating an excluded boundary layer near the walls. The grid spacing was set to 0.2 m between neighbouring sensor points. The grid height was set to 0.85 m in accordance with the daylight standard [35]. The resulting sensor file contained the coordinates of each sensor point together with its surface-normal vector, formatted according to the Radiance sensor-file convention.

2.3.3. Simulation Parameters

A convergence study was performed to establish stable Radiance simulation parameters for the view and daylight matrices and the direct-sun coefficients, independently of the subsequent BSDF-resolution analysis. The study was conducted in two stages. First, the simulation parameters were evaluated using the Three-Phase Method. The selected parameters were then used as the basis for the convergence study of the Five-Phase Method, focusing on the direct-sun coefficients C_{ds}, which involve substantially higher computational demands. The sky resolution for the Three-Phase Method is kept at a minimum of 145 sky patches. For the direct sun coefficient, 5185 suns positions were generated to provide greater angular resolution for the direct-sun contribution. The parameters that are altered are the ambient divisions and the limit weight, which is kept at `1/ad`. The parameters `aa`, `ar`, and `as` are based on those found in the guide to the reference office by MIT [31]. For the Three-Phase Method, the daylight matrix D and the view matrix V are to be calculated. A total of seven simulations were run. The simulation parameters and corresponding run times are listed in Table 4. From the illuminance file, the Daylight Autonomy was calculated with a threshold of 300 lux. The difference between DA_{300} at each point between two consecutive simulations is visualised in Appendix A.1, Figure A1. The difference between two consecutive simulations is reduced when the ambient divisions are increased. The differences decreased with increasing ambient divisions and approached stable values; the parameters from Simulation 7 were therefore selected for the subsequent analyses.

The first part of the convergence study only includes parameters for V and D, but in the Five-Phase Method, we need to include the direct contribution of those parameters, V_d and D_d. It is the same calculation procedure; however, it only calculates the direct contribution, therefore, the parameters for V_d and D_d are based on simulation 7 of the Three-Phase Method. An overview of the chosen parameters is found in Table 5.

Table 4. Simulation parameters for the Three-Phase Method. V is the view matrix and D is the daylight matrix.

		Parameters						Run Time [s]
		ab	**aa**	**ar**	**ad**	**as**	**lw**	
Simulation 1	V	10	0.05	300	1024	20	9.77×10^{-4}	1
	D	5	0.05	300	1024	20	9.77×10^{-4}	26
Simulation 2	V	10	0.05	300	2048	20	4.88×10^{-4}	1
	D	5	0.05	300	2048	20	4.88×10^{-4}	47
Simulation 3	V	10	0.05	300	4096	20	2.44×10^{-4}	2
	D	5	0.05	300	4096	20	2.44×10^{-4}	84
Simulation 4	V	10	0.05	300	8192	20	1.22×10^{-4}	5
	D	5	0.05	300	8192	20	1.22×10^{-4}	158
Simulation 5	V	10	0.05	300	16,384	20	6.10×10^{-5}	10
	D	5	0.05	300	16,384	20	6.10×10^{-5}	310
Simulation 6	V	10	0.05	300	32,768	20	3.05×10^{-5}	19
	D	5	0.05	300	32,768	20	3.05×10^{-5}	612
Simulation 7	V	10	0.05	300	65,536	20	1.53×10^{-5}	32
	D	5	0.05	300	65,536	20	1.53×10^{-5}	1201

Table 5. Parameters used for the view- and daylight matrices for the Three-Phase Method. Includes the direct only contribution of the Three-Phase-Method.

	Parameters					
	ab	**aa**	**ar**	**ad**	**as**	**lw**
V	10	0.05	300	65,536	20	1.53×10^{-5}
D	5	0.05	300	65,536	20	1.53×10^{-5}
V_d	1	0.05	300	65,536	20	1.53×10^{-5}
D_d	0	0.05	300	65,536	20	1.53×10^{-5}

For the convergence study of the direct sun coefficients in the Five-Phase Method, we used point-in-time illuminance results instead of the annual DA_{300}. This is because C_{ds} is the direct contribution and thus very sensitive at certain hours of the year. The seven simulations were run. The parameters for each simulation and the run time are found in Table 6. The point-in-time illuminance results are most sensitive when the direct-light contribution is greatest. Therefore, the hour with the highest mean room illuminance, 6 February at 12:00, was selected for the convergence test and compared with 21 March at 12:00. The differences between the two consecutive simulations are visualised in Appendix A.1, Figures A3 and 11.

Table 6. Parameters for C_{ds} in each simulation.

	Parameters											Run Time [s]
	ab	**aa**	**ar**	**ad**	**as**	**lw**	**dc**	**dt**	**dj**	**st**	**ss**	
Simulation 1	1	0.05	300	8192	20	1.22×10^{-4}	1	0	0	1	0	1668
Simulation 2	1	0.05	300	16,384	20	6.10×10^{-5}	1	0	0	1	0	3212
Simulation 3	1	0.05	300	32,768	20	3.05×10^{-5}	1	0	0	1	0	6413
Simulation 4	1	0.05	300	65,536	20	1.53×10^{-5}	1	0	0	1	0	12,837
Simulation 5	1	0.05	300	131,072	20	7.63×10^{-6}	1	0	0	1	0	25,510
Simulation 6	1	0.05	300	262,144	20	3.81×10^{-6}	1	0	0	1	0	50,819
Simulation 7	1	0.05	300	524,288	20	1.91×10^{-6}	1	0	0	1	0	102,152

Based on the convergence test, we could identify the parameters to use in the Five-Phase method. The pointwise differences between Simulations 6 and 7 had a standard deviation of 692.07 lux. For comparison, the in-between differences on 21 March at 12:00 are visualised in Figure A3, where the differences between simulations were smaller because of the lower direct-light contribution. The results on 6 February at 12:00 for simulations 1–7 are visualised in Figure 11. The results illustrate the influence of the number of ambient divisions, with lower values producing visible sampling artefacts.

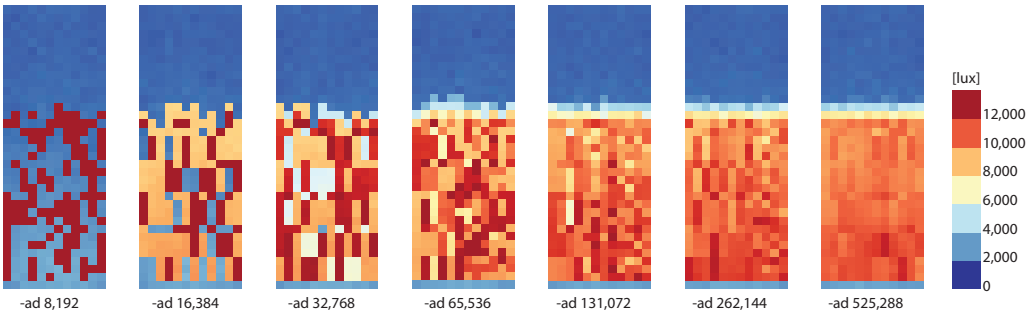


Figure 11. Visualisation of convergence study. Result of simulation 1–7 of the Five-Phase Method (see Table 6). Only the ambient divisions for the direct sun coefficients, C_{ds}, were changed for each simulation. The results show the illuminance on 6 February at 12:00 of a climate-based simulation.

2.3.4. Glazing and Materials

Prior to the simulations, Radiance ".rad" files were created for the room geometry, materials, glazing aperture, and other required model components, together with the sensor-grid file.

The orientation of the glazing-aperture surface normal in the Radiance scene-description Glazing geometry (V-matrix) file (shown as GlazingVmtx.rad) is important because the view matrix is generated by tracing rays from the sensor points towards the glazing surface. If the surface normal is oriented outwards, the glow material will not have any effect, since it is the only light source in the calculation of the view matrix. The two scenarios are shown in Figure 12. The only difference between the two is the arrangement of the four vertices of the glazing polygon, which defines the surface normal orientation.

A Radiance sky and ground glow definition file (`skyglow.rad`) to specify the glow materials and angular discretisation of the sky and ground hemispheres. Here, h = u indicates a uniform hemisphere, and h = r1 indicates the sky discretisation, where the number is the number of subdivisions. For the calculation of the direct-sun coefficients, the BSDF is not applied as an intermediate matrix between the view and daylight matrices. Instead, it is assigned as a BSDF material within the shading-system definition file (`Shade.rad`).

2.4. Data Analysis Methods for the Resolution Sensitivity

To quantify the sensitivity of the simulation results to BSDF resolution, the lower-resolution BSDFs (Klems, TT3, TT4, and TT5) were compared with TT6, corresponding to the highest BSDF resolution investigated in this study. TT6 was therefore used as the numerical reference for the resolution-sensitivity analysis. The resulting deviation metrics quantify numerical differences between the lower-resolution simulations and TT6 and should not be interpreted as measures of absolute prediction accuracy against measured data. With this formulation, a positive MBE indicates that the lower-resolution result is lower than TT6 on average, whereas a negative MBE indicates that it is higher.

```
#objects/GlazingVmtx.rad
#The polygon glowSurface is
oriented inwards.

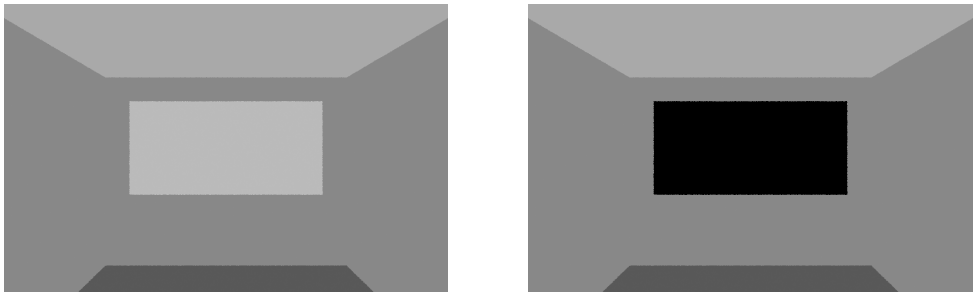
void glow Glazing
0
0
4 1 1 1 0

#@rluxmtx h=kf u=Z
Glazing polygon glowSurface
0
0
12
3.25 −0.05 2.45 #Point 1
3.25 −0.05 1.05 #Point 2
0.35 −0.05 1.05 #Point 3
0.35 −0.05 2.45 #Point 4
```

```
#objects/GlazingVmtx.rad
#The polygon glowSurface is
oriented outwards.

void glow Glazing
0
0
4 1 1 1 0

#@rluxmtx h=kf u=Z
Glazing polygon glowSurface
0
0
12
3.25 −0.05 2.45 #Point 1
0.35 −0.05 2.45 #Point 2
0.35 −0.05 1.05 #Point 3
3.25 −0.05 1.05 #Point 4
```



(**a**) (**b**)

Figure 12. Effect of the glazing-aperture surface-normal orientation: (**a**) inward-facing surface normal and (**b**) outward-facing surface normal. The views were generated using Radiance geometry preview (`objview`). Because the surface with the applied glow material is the only light source used to calculate the view matrix, the outward-facing configuration in (**b**) receives no light. The colours are used to distinguish the orientation of the glazing surface and do not represent quantitative simulation results.

For a set of n paired observations, y_i denotes the TT6 reference value and x_i denotes the corresponding value obtained using a lower-resolution BSDF. Four measures of deviation were calculated: Mean Absolute Error (MAE), Mean Bias Error (MBE), Root Mean Square Error (RMSE), and Normalised Root Mean Square Error (NRMSE).

The MAE quantifies the mean magnitude of the deviation from TT6 and is defined as:

$$\mathrm{MAE} = \frac{1}{n}\sum_{i=1}^{n}|y_i - x_i|. \tag{2}$$

The MBE represents the mean signed deviation between the lower-resolution and TT6 results and is defined as:

$$\mathrm{MBE} = \frac{1}{n}\sum_{i=1}^{n}(y_i - x_i). \tag{3}$$

Unlike MAE, MBE retains the direction of the deviation and therefore indicates whether the lower-resolution results are systematically higher or lower than the corresponding TT6 results.

The RMSE represents the quadratic mean of the deviations and is defined as:

$$\mathrm{RMSE} = \sqrt{\frac{1}{n}\sum_{i=1}^{n}(y_i - x_i)^2}. \tag{4}$$

RMSE is non-negative, with a value of zero indicating no deviation from TT6. Lower RMSE values therefore indicate closer numerical agreement with the TT6 reference.

To facilitate comparison between quantities and shading configurations with different numerical scales, RMSE was normalised by the range of the corresponding TT6 reference data:

$$\mathrm{NRMSE} = \frac{\mathrm{RMSE}}{y_{\max} - y_{\min}}, \tag{5}$$

where $y_{\max}$ and $y_{\min}$ are the maximum and minimum values, respectively, of the corresponding TT6 reference dataset. The normalisation was performed separately for each shading configuration and evaluated quantity, such that all lower-resolution BSDFs within a given comparison were normalised using the same TT6 range. A lower NRMSE therefore indicates closer agreement with TT6 relative to the range of the corresponding reference data.

```
#skyDomes/skyglow.rad      #blinds/Shade.rad
#@rfluxtmtx u=+Y h=u
void glow groundglow       void BSDF Shade
0                          6 0 blinds/Shade_1A_TT_6.xml 0 0 1 .
0                          0
4 1 1 1 0                  0

groundglow source ground   Shade polygon glazing
0                          0
0                          0
4 0 0 -1 180               12
                           3.25 -0.05 2.45
#@rfluxmtx u=+Y h=r1       3.25 -0.05 1.05
void glow skyglow          0.35 -0.05 1.05
0                          0.35 -0.05 2.45
0
4 1 1 1 0

skyglow source skydome
0
0
4 0 0 1 180
```

Together, these metrics provide complementary measures of the magnitude, direction, and scale-normalized extent of the deviations associated with BSDF resolution.

3. Results

The results obtained using Klems, TT3, TT4, and TT5 BSDFs were compared with TT6, which serves as the highest-resolution numerical reference in this study. Comparisons were performed for both point-in-time illuminance and climate-based daylight metrics. MAE, MBE, RMSE, and NRMSE were used to quantify deviations from TT6. Sensitivity to BSDF resolution was also compared across the different shading-system variations, with MAE expressing deviation in the units of the simulated quantity and NRMSE providing a normalised measure for comparison across cases.

3.1. Analysis of Deviation Metrics in Point-in-Time Calculations

The point-in-time evaluation was performed for the hour with the highest average room illuminance for each shading system. The hour was selected independently of the subsequent comparison between BSDF resolutions; selecting the hour based on maximum MAE or local deviation would instead make the selection criterion dependent on the differences being investigated. The selected hour for each solar shading system is shown in Table 7.

Table 7. Month, Date, time and hour of the year (HOY) for point-in-time simulations.

Shading	Month	Day	Time	HOY	Solar Angle
1A	February	6	12:00	876	18.5°
1B	November	27	11:00	7931	12.0°
2A	November	27	11:00	7931	12.0°
2B	December	29	12:00	8700	11.0°
3	February	6	12:00	876	18.5°
4A	February	6	12:00	876	18.5°
4B	February	6	12:00	876	18.5°

For each of the instances shown in Table 7, Figure 13a–g show the illuminance distribution across the room depth. It can be seen that the general trend across all shading types is a gradual decrease in illuminance with increasing distance from the window, as expected. However, the rate of decrease and absolute illuminance values vary significantly depending on the shading system and BSDF resolution. The Klems method consistently underestimates illuminance levels, especially near the window (0 to 3 m range). This is particularly evident for Shade_3, Shade_4A, and Shade_4B. TT3 generally overestimates illuminance compared to TT6, but its behaviour varies depending on the shading system. For shading configurations with a high degree of sunlight penetration, deviations are largest near the window, where direct sunlight is strongest. The observed trend indicates greater sensitivity to BSDF resolution in high-transmission shading systems, whereas more obstructive systems show smaller deviations between resolutions. Illuminance deviations are most significant near the window, where direct sunlight penetration is misrepresented particularly when low-resolution BSDFs are used. In deeper parts of the room, illuminance values stabilise, but discrepancies between lower and higher BSDF resolutions remain noticeable. The transition from direct-sun areas to fully shaded regions is not well captured by lower-resolution BSDFs, as seen in the plots where TT3 and Klems deviate significantly from TT6. For many shading types, TT6 generally aligns well with TT5, suggesting that beyond a certain resolution (TT5 and above), further increases in BSDF resolution do not substantially change the simulated illuminance distribution. These findings align with the deviation metrics in Table 8, which compiles key deviation metrics—MAE, MBE, RMSE and NRMSE—for various shading system configurations at different BSDF resolution settings; see also Figure 14a–g. These results show that the larger deviations from TT6 occur for shading systems with strong direct daylight contributions. Notably, the Venetian blinds, Shade_1A (Figure 14a) and Shade_1B (Figure 14b), show pronounced variations depending on the solar angle, while the mesh-based systems, Shade_4A (Figure 14e), Shade_4B (Figure 14f), and Shade_3 (Figure 14g), show larger deviations due to their directional scattering properties.

To extend these findings to an annual representation, temporal maps illustrate the Mean Absolute Error (MAE) for each hour across all sensor points compared to TT6 (Figures A4–A10 in Appendix A.2). The results indicate that shading systems allowing greater direct daylight penetration exhibit larger deviations from TT6, as seen in Shade_3

(Figure A8), Shade_4A (Figure A9), and Shade_4B (Figure A10). This trend aligns with expectations, given that BSDFs are used to calculate direct daylight in the Five-Phase Method.

Across all shading types, MAE consistently decreases from TT3 and Klems to TT4, with the lowest values for TT5, as summarised in Table 8. Venetian blinds exhibit distinct seasonal variations in MAE due to their cutoff angles and geometry, unlike mesh shading systems. For Venetian blinds, April to September shows minimal MAE, with the exception of Shade_1A, where noticeable deviations appear mainly for TT3 and towards the end of September. Shade_2A follows a similar trend but with less pronounced deviations.

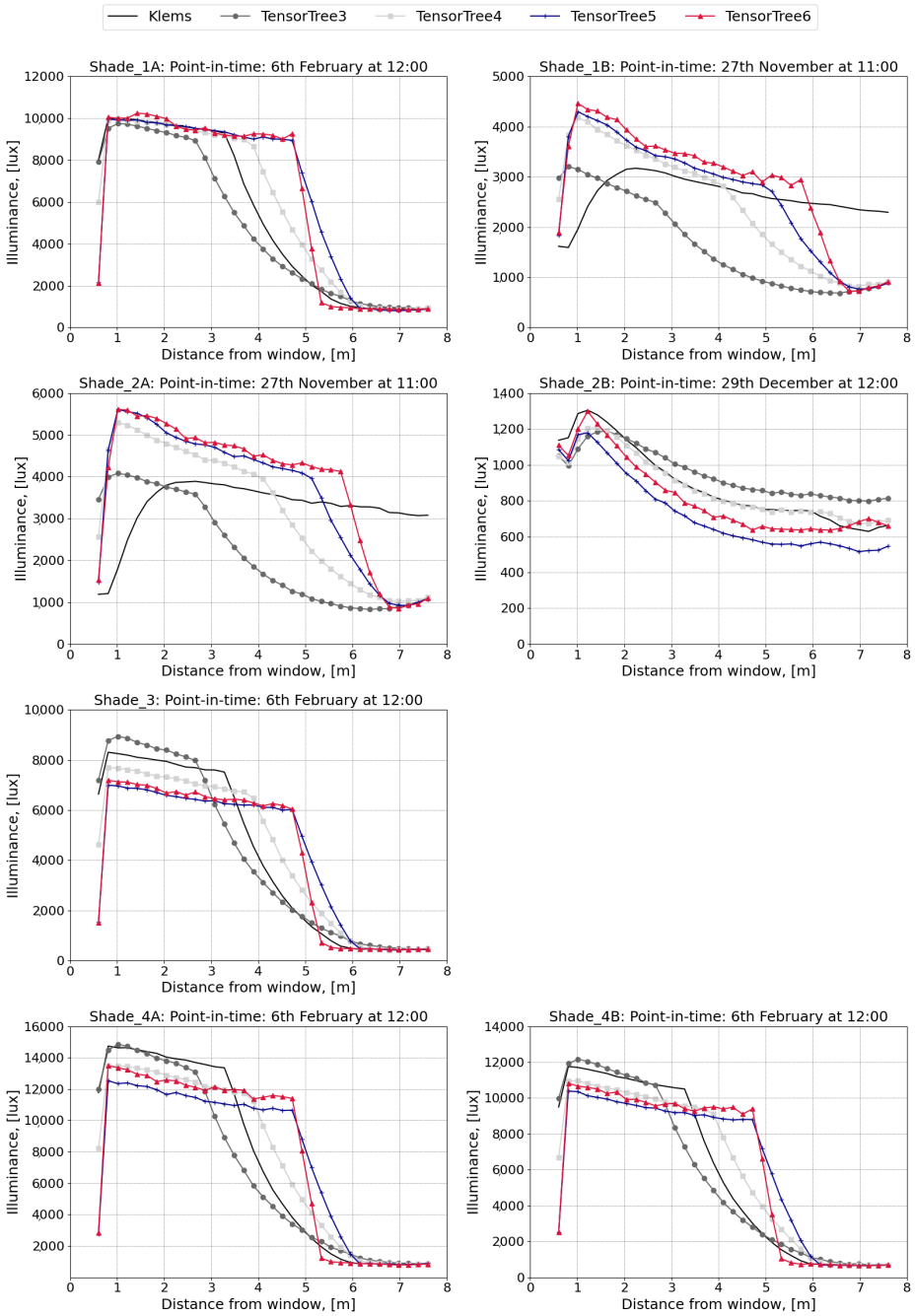


Figure 13. Average illuminance [lux] for grid points in a distance from the window [m].

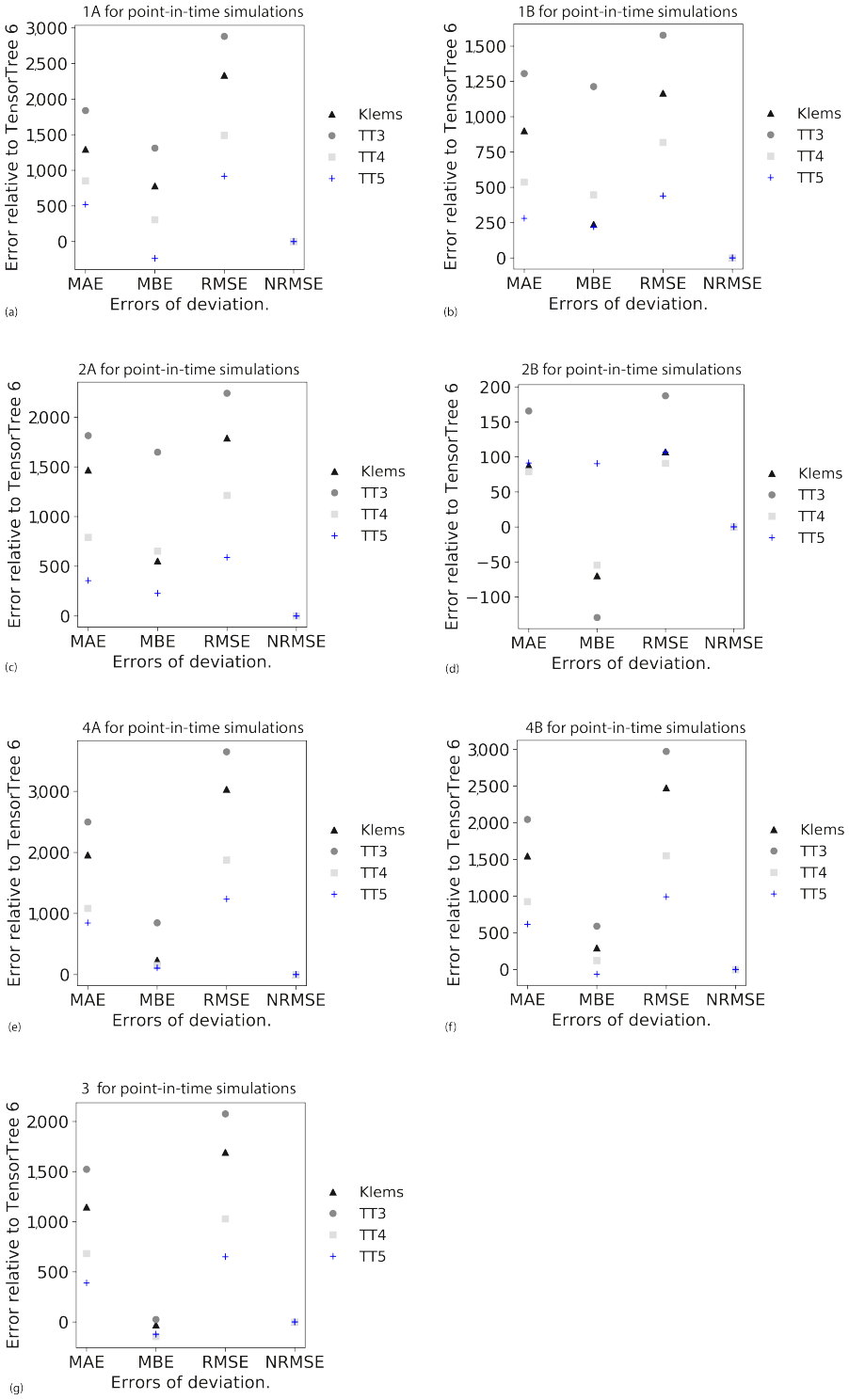


Figure 14. Deviation metrics relative to TT6 for point-in-time simulations of each shading system: (**a**) Shade_1A, (**b**) Shade_1B, (**c**) Shade_2A, (**d**) Shade_2B, (**e**) Shade_4A, (**f**) Shade_4B, and (**g**) Shade_3.

Table 8. Deviation metrics relative to TT6 for each shading system.

Shadings	Deviation	Klems	TT3	TT4	TT5
Shading System 1A	MAE	1296.1	1839.6	851.1	520.5
	MBE	781.3	1312.1	305.3	−238.3
	RMSE	2336.7	2881	1490.4	916.4
	NRMSE	0.25	0.31	0.16	0.09

Table 8. *Cont.*

Shadings	Deviation	Klems	TT3	TT4	TT5
Shading System 1B	MAE	900.9	1305.5	537.1	279.9
	MBE	238.2	1213.1	446.8	219.3
	RMSE	1167.3	1577.0	818.5	439.0
	NRMSE	0.40	0.56	0.22	0.11
Shading System 2A	MAE	1467.8	1814.2	790.3	355.1
	MBE	554.1	1647.5	653.3	226.6
	RMSE	1790.3	2240.4	1213.0	588.7
	NRMSE	0.47	0.63	0.25	0.11
Shading System 2B	MAE	87.9	165.6	78.9	91.4
	MBE	−69.7	−129.4	−54.6	90.4
	RMSE	107.4	187.3	90.9	106.8
	NRMSE	0.12	0.22	0.10	0.11
Shading System 3	MAE	1146.7	1522.7	683.1	389.2
	MBE	−28.8	25.4	−145.9	−122.6
	RMSE	1692.6	2075.6	1028.4	649.5
	NRMSE	0.21	0.24	0.14	0.10
Shading System 4A	MAE	1958.7	2498.4	1082.8	844.9
	MBE	235.5	846.8	145.4	104.6
	RMSE	3036.0	3648.9	1875.9	1235.1
	NRMSE	0.21	0.25	0.14	0.10
Shading System 4B	MAE	1547.9	2045.5	924.1	616.1
	MBE	294.1	590.4	121.3	−64.5
	RMSE	2476.1	2972.4	1550.5	990.3
	NRMSE	0.22	0.25	0.15	0.10

Angled Venetian blinds demonstrate lower MAE values than their non-angled counterparts due to reduced direct daylight penetration. Shade_2A, with a cutoff angle of 25°, shows minimal MAE, consistent with the reduced direct daylight penetration associated with its higher cutoff angle.

In summary, shading systems with greater direct daylight penetration exhibit larger deviations, as evident in the annual MAE maps.

3.2. Analysis of Deviation Metrics in Climate-Based Metrics Calculations

The effect of BSDF resolution on annual daylight metrics was relatively small, indicating that lower-resolution BSDFs can provide results close to TT6. Across all shading systems, the largest deviations from TT6 are summarised in Table 9 and illustrated in Figure 15.

Table 9. Maximum deviations for different daylight metrics compared to TT6.

Metric	MAE	MBE	RMSE	NRMSE
DA_{300}	0.76	−0.62	0.98	0.04
cDA_{300}	0.53	−0.43	0.69	0.01
$UDI_{100–3000}$	0.67	−0.36	1.09	0.02

These values suggest that the investigated annual daylight metrics show relatively small sensitivity to BSDF resolution, meaning that lower-resolution BSDFs (TT3–TT5) may still be suitable for daylight simulations with only small deviations from TT6.

For cDA_{300} the results suggest that its partial-credit approach may contribute to the smaller deviations observed between BSDF resolutions. This is evident when comparing

Shade_1A and Shade_2A to Shade_1B and Shade_2B, where higher cutoff angles were associated with smaller deviations from TT6. A similar pattern is observed between Shade_4A and Shade_4B, where the differences in the amount and type of light transmission between these two shading systems are minimal, resulting in negligible deviations in DA_{300} and cDA_{300}. The same holds true for $UDI_{100–3000}$, further reinforcing the conclusion that BSDF resolution has little impact on annual daylight metrics. For Shade_4B, the smallest deviation from TT6 occurred for TT3, showing that, for certain shading conditions, a lower-resolution BSDF can also show close agreement with TT6.

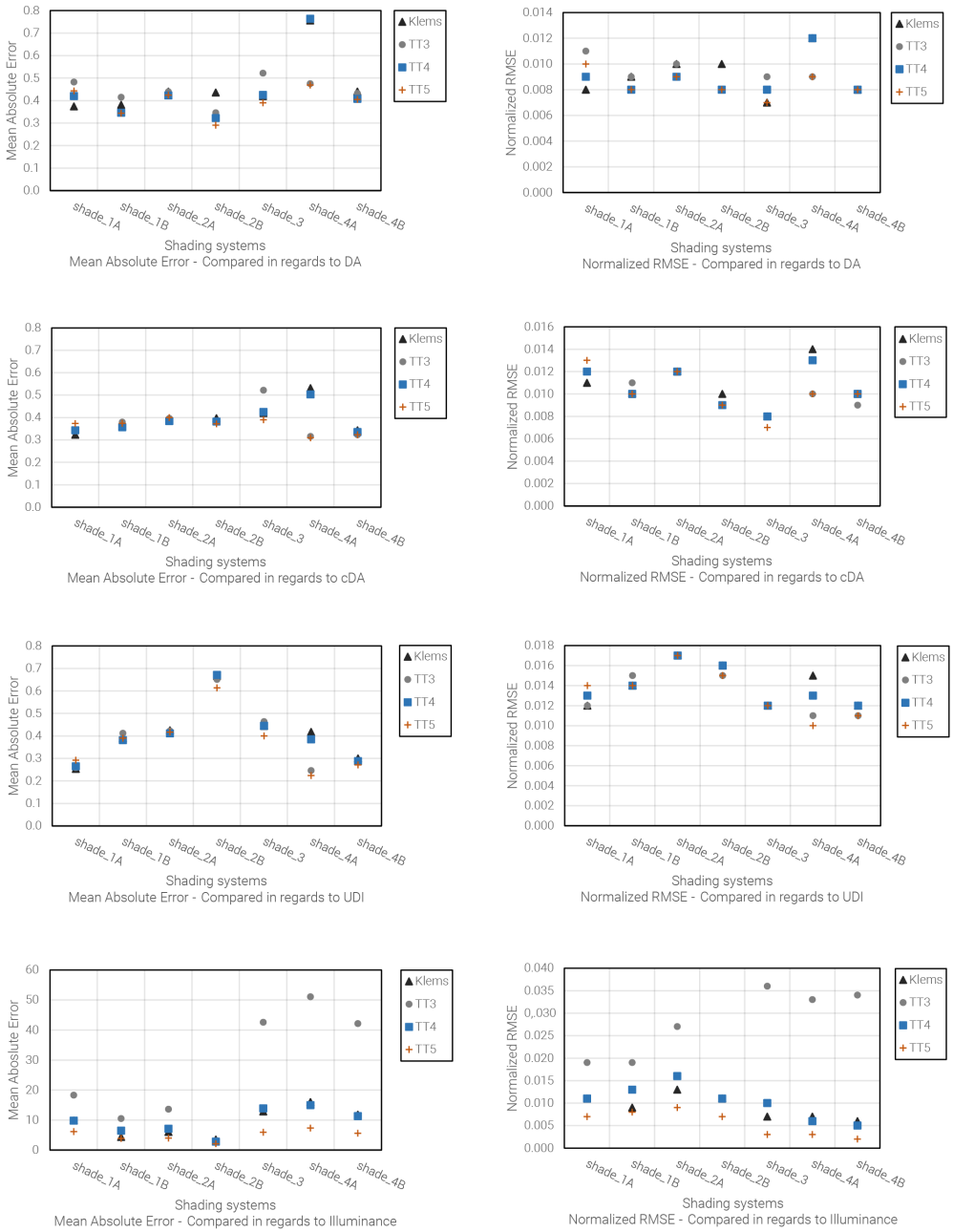


Figure 15. Comparison of MAE and NRMSE for all shading systems. Annual climate-based simulations.

A clear distinction between BSDF resolutions becomes apparent when analysing illuminance values. Among all shading types:

- TT5 shows the closest agreement with TT6, as indicated by all deviation metrics.

- TT4 and Klems show similar deviation, showing comparable NRMSE values across most shading systems, except for Shade_2A, where a noticeable discrepancy arises.
- TT3 shows the largest deviations, particularly in shading systems with lower shading factors, such as Shade_3, Shade_4A, and Shade_4B, where its deviation from TT6 is most pronounced.

Overall, BSDF resolution had a relatively small influence on the investigated annual daylight metrics (DA_{300}, cDA_{300}, and $UDI_{100–3000}$), with TT4 and TT3 showing only small deviations from TT6. In contrast, point-in-time illuminance was more sensitive to BSDF resolution: TT5 consistently showed the closest agreement with TT6, while TT3 showed larger deviations, particularly for shading systems with lower shading factors.

3.3. Sensitivity of BSDF Resolution in Shading Systems

Table 10 compares the deviation measures (MAE, MBE, RMSE, NRMSE) across all shading systems and BSDF resolutions. The results show that sensitivity to BSDF resolution varies with both the daylight metric and shading-system characteristics. Across all shading systems, the maximum deviations from TT6 for DA_{300} were 0.76 (MAE), −0.62 (MBE), 0.98 (RMSE), and 0.04 (NRMSE). For cDA_{300}, the corresponding values were 0.53 (MAE), −0.43 (MBE), 0.69 (RMSE), and 0.01 (NRMSE). For $UDI_{100–3000}$, they were 0.67 (MAE), −0.36 (MBE), 1.09 (RMSE), and 0.02 (NRMSE). These values indicate that lower BSDF resolutions can be used for annual illuminance-based metrics with only small deviations from TT6.

Considering the deviations in DA_{300} and cDA_{300}, the results suggest that the partial-credit approach used in cDA_{300} may contribute to the smaller deviations observed for shading systems with higher cutoff angles, as seen when comparing Shade_1A and Shade_2A with Shade_1B and Shade_2B. A similar pattern of small deviations is observed for Shade_4A and Shade_4B. The resulting differences in DA_{300} and cDA_{300} are therefore small. $UDI_{100–3000}$ also showed small differences between BSDF resolutions; however, this metric is calculated differently, based on the proportion of occupied time for which illuminance falls within the specified 100–3000 lx range. Its low sensitivity to BSDF resolution should therefore not be attributed to the partial-credit mechanism of cDA_{300}.

Table 10. Deviation metrics relative to TT6 for all shading systems and BSDF resolutions.

		DA_{300}				cDA_{300}				$UDI_{100–3000}$				Illuminance			
		Klems	**TT3**	**TT4**	**TT5**	**Klems**	**TT3**	**TT4**	**TT5**	**Klems**	**TT3**	**TT4**	**TT5**	**Klems**	**TT3**	**TT4**	**TT5**
Shading System 1A	MAE	0.37	0.48	0.42	0.44	0.32	0.34	0.34	0.37	0.25	0.26	0.27	0.29	9.87	18.32	9.79	6.16
	MBE	−0.04	−0.22	−0.05	−0.02	0.02	−0.09	0.01	0.02	0.02	−0.02	0.02	0.03	4.72	15.30	7.88	2.57
	RMSE	0.54	0.74	0.62	0.67	0.49	0.53	0.53	0.58	0.40	0.42	0.43	0.45	12.66	21.41	12.34	7.96
	NRMSE	0.01	0.01	0.01	0.01	0.01	0.01	0.01	0.01	0.01	0.01	0.01	0.01	0.01	0.02	0.01	0.01
Shading System 1B	MAE	0.38	0.42	0.35	0.34	0.37	0.38	0.36	0.37	0.39	0.41	0.38	0.39	4.38	10.49	6.44	3.86
	MBE	−0.13	−0.11	−0.04	−0.01	−0.05	−0.07	−0.03	−0.00	0.00	−0.01	0.03	0.04	−0.44	9.10	5.54	2.16
	RMSE	0.59	0.61	0.51	0.51	0.54	0.54	0.52	0.53	0.62	0.66	0.62	0.62	5.99	12.65	8.97	5.20
	NRMSE	0.01	0.01	0.01	0.01	0.01	0.01	0.01	0.01	0.01	0.02	0.01	0.01	0.01	0.02	0.01	0.01
Shading System 2A	MAE	0.44	0.44	0.42	0.42	0.39	0.40	0.38	0.40	0.43	0.42	0.41	0.42	6.00	13.61	7.09	3.99
	MBE	−0.14	−0.08	−0.03	0.02	−0.09	−0.08	−0.06	−0.03	−0.08	−0.05	−0.06	−0.04	0.09	11.32	5.93	1.53
	RMSE	0.61	0.60	0.58	0.60	0.56	0.57	0.55	0.58	0.68	0.68	0.68	0.70	8.14	16.19	9.28	5.17
	NRMSE	0.01	0.01	0.01	0.01	0.01	0.01	0.01	0.01	0.02	0.02	0.02	0.02	0.01	0.03	0.02	0.01
Shading System 2B	MAE	0.44	0.35	0.32	0.29	0.40	0.38	0.38	0.37	0.67	0.65	0.67	0.61	3.52	3.05	2.82	2.09
	MBE	−0.30	−0.05	−0.03	−0.06	−0.16	−0.02	−0.02	−0.06	−0.17	−0.07	−0.11	−0.11	−3.27	−1.09	−0.96	0.50
	RMSE	0.55	0.49	0.45	0.44	0.54	0.52	0.51	0.50	1.09	1.06	1.08	1.00	4.21	4.57	4.29	2.77
	NRMSE	0.01	0.01	0.01	0.01	0.01	0.01	0.01	0.01	0.02	0.02	0.02	0.02	0.01	0.01	0.01	0.01
Shading System 3	MAE	0.42	0.52	0.43	0.39	0.35	0.37	0.36	0.33	0.44	0.46	0.45	0.40	12.87	42.57	13.89	5.93
	MBE	−0.15	−0.32	−0.15	−0.06	−0.05	−0.11	−0.10	−0.02	−0.04	−0.02	−0.06	−0.01	8.54	36.50	6.81	−0.27
	RMSE	0.62	0.73	0.65	0.61	0.52	0.56	0.55	0.50	0.79	0.78	0.77	0.74	27.19	115.32	34.93	9.75
	NRMSE	0.01	0.01	0.01	0.01	0.01	0.01	0.01	0.01	0.01	0.01	0.01	0.01	0.01	0.04	0.01	0.004
Shading System 4A	MAE	0.76	0.48	0.76	0.47	0.53	0.32	0.50	0.31	0.42	0.25	0.39	0.22	15.99	51.11	14.94	7.34
	MBE	−0.62	−0.01	−0.62	0.02	−0.43	0.002	−0.40	0.02	−0.36	0.01	−0.31	0.02	−9.98	47.60	−7.96	0.82
	RMSE	0.96	0.74	0.98	0.75	0.69	0.52	0.67	0.53	0.54	0.39	0.50	0.37	25.39	110.69	22.20	10.04
	NRMSE	0.01	0.04	0.01	0.01	0.01	0.01	0.01	0.01	0.02	0.01	0.01	0.01	0.01	0.03	0.01	0.003
Shading System 4B	MAE	0.44	0.43	0.41	0.41	0.34	0.32	0.34	0.32	0.30	0.29	0.29	0.27	11.79	42.16	11.29	5.60
	MBE	−0.10	−0.12	−0.10	−0.03	−0.03	−0.05	−0.06	−0.03	−0.01	−0.02	−0.02	−0.02	8.11	39.02	6.65	−0.46
	RMSE	0.67	0.66	0.61	0.66	0.56	0.51	0.54	0.52	0.52	0.49	0.52	0.49	18.56	96.24	17.17	7.54
	NRMSE	0.01	0.01	0.01	0.01	0.01	0.01	0.01	0.01	0.01	0.01	0.01	0.01	0.01	0.03	0.01	0.003

Note: Red shading highlights selected cases exhibiting relatively large deviations from the TT6 reference.

3.3.1. Impact of Different Metrics on Resolution Sensitivity

The impact of BSDF resolution varies across different daylight performance metrics. Annual daylight metrics, including DA_{300}, cDA_{300}, and $UDI_{100–3000}$, exhibit relatively minor variations across different BSDF resolutions. This suggests that lower-resolution BSDFs, such as TT3 and TT4, show only small deviations from TT6 for the investigated annual daylight metrics. In contrast, illuminance-based calculations are considerably more sensitive to BSDF resolution. Shading systems such as Shade_3 and Shade_4A show notably higher deviations when computed using TT3 compared to TT5. In these cases, the MAE and RMSE obtained with TT3 are up to four times those obtained with TT5, indicating substantially closer agreement with TT6 at the higher BSDF resolution. These findings highlight the importance of selecting an appropriate BSDF resolution based on the specific daylight performance metric being evaluated.

3.3.2. Cutoff Angles and Deviation Patterns

The deviation pattern varies with the shading-system configuration and corresponding cut-off angle. For the Venetian-blind variants, the configurations with higher cut-off angles (Shade_1A and Shade_2A) generally showed smaller deviations from TT6 than the corresponding lower-cut-off-angle configurations (Shade_1B and Shade_2B). For cDA_{300}, its partial-credit approach may contribute to the relatively small deviations observed between BSDF resolutions. Among the investigated Venetian-blind systems, Shade_2A showed relatively small deviations. Its configuration restricts direct daylight penetration more strongly than Shade_2B, which may contribute to the smaller MAE and RMSE observed. These results indicate an association between shading-system configuration, directional light transmission and sensitivity to BSDF resolution.

3.3.3. Agreement Across BSDF Resolutions

The comparison of BSDF resolutions, based on the deviation metrics in Table 10, shows that TT5 consistently provides the closest agreement with TT6 across the investigated shading systems. TT4 and Klems show similar deviations, particularly in DA_{300} and cDA_{300}, where their NRMSE values remain comparable across most shading systems. On the other hand, TT3 exhibits the largest deviations from TT6, especially in shading systems with lower shading factors, such as Shade_3, Shade_4A, and Shade_4B. These findings indicate that while lower-resolution BSDFs can still be used for certain annual daylight metrics, higher resolutions such as TT5 provides closer agreement with TT6 in point-in-time illuminance analyses.

3.4. BSDF Generation Time

Table 11 presents the BSDF generation time, in hours, for each shading system and BSDF resolution. The results show that Klems, TT3, and TT4 have relatively similar generation times, with TT3 requiring the shortest generation time. In contrast, TT5 requires substantially more generation time than Klems, TT3, and TT4, although its generation time is approximately 75% lower than that of TT6. This trend is consistent with the increasing number of regions at successive tensor-tree levels, which results in a substantial increase in computational demand.

Considering the annual simulation results, the use of lower-resolution BSDFs offers a substantial reduction in processing time while maintaining results comparable to high-resolution BSDFs. This can significantly reduce waiting time for consultants and minimise computational resource demands. The relatively small differences in generation time between Klems, TT3, and TT4 suggest that choosing a slightly higher-resolution BSDF could

reduce deviations from TT6 without excessive delays, particularly if minor computational upgrades are implemented.

Table 11. Duration of BSDF generation [hours].

	Klems	TT3	TT4	TT5	TT6
Shade 1A	2.0	0.7	2.9	11.8	47.1
Shade 1B	2.1	0.8	3.2	12.7	50.9
Shade 2A	2.6	1.0	3.9	16.7	63.0
Shade 2B	2.7	1.1	4.1	16.3	66.1
Shade 3	1.4	0.5	2.1	8.1	32.5
Shade 4A	0.9	0.3	1.3	5.1	20.6
Shade 4B	1.4	0.5	2.1	8.2	32.9
Avg	1.9	0.7	2.8	11.3	44.7

In contrast, results from point-in-time simulations indicate significant differences between BSDFs of varying resolutions. Higher-resolution BSDFs provide increased precision in daylight analysis, particularly for evaluating dynamic daylit spaces. However, designers could still benefit from lower-resolution BSDFs if they are aware of how results may shift when using higher resolutions. This understanding could enable efficient design processes while balancing computational efficiency and resolution sensitivity.

4. Discussion

The results from the illuminance distributions, deviation analysis, and climate-based daylight metrics demonstrate that sensitivity to BSDF resolution depends strongly on the type of assessment. Across the investigated shading systems, increasing BSDF resolution generally reduced deviations from TT6, with TT5 showing close agreement with the highest-resolution numerical reference. Climate-based metrics such as DA_{300}, cDA_{300}, and $UDI_{100–3000}$ showed relatively small variations across BSDF resolutions. This indicates that higher BSDF resolution becomes particularly relevant for detailed point-in-time illuminance assessments, whereas lower-resolution BSDFs, such as TT4 or Klems, may be sufficient for annual illuminance-based daylight performance evaluations under the conditions investigated.

4.1. BSDF Resolution and Deviation Patterns

The impact of BSDF resolution is most evident in shading systems that permit substantial direct daylight penetration. Shade_3, Shade_4A, and Shade_4B exhibited the highest MAE values, particularly near the window, indicating that deviations are most pronounced in scenarios with strong directional light transmission. The Five-Phase Method relies on BSDFs for direct daylight calculations, and the observed spatial deviations may therefore be influenced by the lower angular resolution used to represent directional transmission through complex fenestration systems. Lower-resolution BSDFs show the largest deviations near the window, coinciding with regions where direct-light effects are strongest. The direction of the deviation, however, differs between BSDF resolutions and shading systems. Klems generally underestimates illuminance relative to TT6, whereas TT3 more frequently overestimates illuminance near the window. This suggests that lower-resolution BSDFs may represent the spatial distribution of directional light transmission through the CFS with less detail, as the transmission is distributed into larger, discretised patches.

4.2. Shading Type and Deviation Trends

The sensitivity to BSDF resolution varies with shading geometry and optical properties. The Venetian-blind systems (Shade_1A, Shade_1B, Shade_2A, and Shade_2B) generally show smaller deviations across BSDF resolutions than Shade_3, Shade_4A, and Shade_4B. This may be associated with differences in their directional light-transmission characteristics. However, deviations are still most pronounced at lower solar angles, where more direct sunlight reaches the interior. Mesh-based shading systems (Shade_3, Shade_4A, Shade_4B) exhibit greater sensitivity to BSDF resolution, which may be associated with their greater direct daylight transmission. In the investigated cases, systems allowing greater direct daylight penetration showed larger MAE deviations. The results generally show decreasing deviations from TT6 with increasing BSDF resolution, although the magnitude of this effect varies between shading systems. TT5 shows relatively close agreement with TT6, whereas Klems and TT3 show larger deviations for systems with strong directional daylight transmission.

4.3. Spatial Distribution of Deviations

The magnitude of the deviations also varies with position within the room. Near the window, lower-resolution BSDFs show the largest deviations, particularly in regions where direct-light effects are strongest. Klems generally underestimates illuminance relative to TT6, whereas TT3 more frequently overestimates it. In the middle zone of the room, discrepancies between BSDF resolutions decrease, but TT3 still shows larger deviations from TT6. In deeper parts of the room, the differences between TT5 and TT6 become small, suggesting diminishing sensitivity to further increases in BSDF resolution in regions dominated by indirect light.

4.4. Implications from Climate-Based Simulations

Point-in-time simulations provide valuable insights into BSDF resolution sensitivity under specific daylight conditions. In contrast, climate-based annual simulations account for time-varying sky and solar conditions across the year, rather than evaluating a single specified condition.

The results from climate-based metrics such as DA_{300}, cDA_{300}, and $UDI_{100–3000}$ indicate that BSDF resolution has a relatively minor influence on the investigated annual daylight metrics. TT3 and Klems show relatively small deviations from TT6 for most shading systems and may therefore be sufficient for annual evaluations under the investigated conditions. However, for systems with greater direct daylight penetration, such as Shade_3, Shade_4A, and Shade_4B, lower-resolution BSDFs show notable deviations in localised illuminance values, reinforcing the findings from point-in-time simulations. These results suggest that while higher-resolution BSDFs (TT5 or TT6) are more important for representing detailed point-in-time illuminance distributions, lower-resolution BSDFs may be sufficient for annual daylight performance evaluations under the conditions investigated.

4.5. Transferability to Luminance-Based Metrics

The present study focused specifically on illuminance-based evaluations. The results should therefore not be directly transferred to luminance-based metrics, particularly daylight glare metrics such as DGP. Even high-resolution BSDFs require careful consideration for glare assessment, as the small angular extent of the sun (approximately $\times 0.5$ degrees in diameter) is difficult to resolve adequately. At the same time, small, high-luminance sources can have an important influence on glare metrics. The influence of BSDF resolution and glare-source size on metrics such as DGP therefore requires further investigation. The scope of the study should also be considered when interpreting the findings. The seven

configurations represent commonly used shading systems with different geometrical and light-transmission characteristics, but not the full diversity of complex fenestration systems. A single reference-room orientation and climate were maintained as controlled conditions, while the annual simulations captured variations in solar position throughout the year. Finally, TT6 represents the highest-resolution numerical reference considered, rather than experimentally validated ground truth.

5. Conclusions

This study investigated the impact of BSDF resolution on daylight simulations for seven representative shading systems using both annual climate-based and point-in-time analyses. The results show that BSDF resolution has a relatively small influence on the investigated annual daylight metrics, whereas larger deviations occur in point-in-time calculations, particularly for shading systems allowing greater direct sunlight penetration.

Shading configurations such as Shade_3, Shade_4A, and Shade_4B exhibited the largest deviations, particularly near the window, where direct-light effects are strongest. TT5 showed close agreement with TT6 across different room depths, reinforcing the importance of resolution selection based on the specific daylighting scenario.

Climate-based simulations further show that lower-resolution BSDFs may be sufficient for the investigated annual daylight metrics (DA_{300}, cDA_{300}, and $UDI_{100–3000}$), for which deviations from TT6 remained relatively small. However, for detailed point-in-time illuminance assessments involving strong directional or direct-solar transmission, higher-resolution BSDFs such as TT5 provide closer agreement with TT6.

This study focused on illuminance-based evaluations and did not investigate the influence of BSDF resolution on glare. As discussed in Section 4.5, the present findings should therefore not be directly transferred to luminance-based metrics such as Daylight Glare Probability (DGP). Previous work has investigated approaches for addressing limitations associated with the representation of specular and near-specular transmission [24,36]; however, further research is required to determine the BSDF resolution requirements for glare assessment.

Moreover, the present study considered static shading configurations. Future work could extend the analysis to automated and adaptive façade systems to investigate BSDF resolution requirements under dynamically changing shading conditions.

The findings also indicate the potential for resolution-specific simulation workflows, in which lower-resolution BSDFs are used for annual daylight assessments and higher-resolution BSDFs, such as TT5, are used for detailed point-in-time analyses. Such an approach could reduce computational demand while retaining the level of angular detail required for the simulation objective.

From a practical perspective, the appropriate BSDF resolution depends on the simulation objective. While TT6 represents the highest-resolution numerical reference investigated, TT5 generally showed close agreement with TT6 while requiring substantially less BSDF-generation time. Lower-resolution BSDFs such as TT4 or Klems may therefore be sufficient for annual illuminance-based assessments under the investigated conditions, whereas TT5 is preferable for detailed point-in-time assessments involving strong directional or direct-solar transmission.

The findings should be interpreted within the scope of the study. The seven configurations represent commonly used shading systems with different geometrical and light-transmission characteristics, but not the full diversity of complex fenestration systems. A single reference-room orientation and climate were maintained as controlled conditions, while the annual simulations captured variations in solar position throughout the year. TT6

represents the highest-resolution numerical reference considered rather than experimentally validated ground truth.

The present study identified the largest spatial deviations in regions associated with strong directional light transmission; however, the individual contributions of direct-sun, diffuse-sky and interreflection components were not separately evaluated. Future work could decompose the simulated illuminance into these components to determine their relative sensitivity to BSDF resolution and further investigate the mechanisms underlying the observed spatial deviations.

Moreover, future work should extend the established framework to a broader range of shading and complex fenestration systems to further examine the generalisability of the observed resolution sensitivities. Further investigations across different orientations and climatic conditions, together with experimental validation against measured illuminance, would provide additional evidence for the transferability and absolute predictive accuracy of the approach.

Author Contributions: M.S.K.: Writing—review & editing, Conceptualization, Supervision, Project Investigation. M.K.P.: Writing—original draft, Investigation, Coding and development, Formal Analysis. F.R.: Writing—original draft, Investigation, Formal Analysis. E.M.B.: Review & Editing, Visualisation. D.G.-M.: Writing—review & editing, Validation, Supervision. All authors have read and agreed to the published version of the manuscript.

Funding: The authors express their gratitude to the Bjarne Saxhof Fonden for their support in facilitating the studies.

Informed Consent Statement: Not applicable.

Data Availability Statement: The data that support the findings of this study are available from the corresponding author upon reasonable request.

Acknowledgments: The research was conducted within the framework of an MSc thesis authored by Mikkel K. Pedersen and Frederik Rasmussen and a BSc thesis by Emil P. O. Kjeldsen.

Conflicts of Interest: Author Mikkel Kofod Pedersen was employed by the company Ladybug Tools LLC. The remaining authors declare that the research was conducted in the absence of any commercial or financial relationships that could be construed as a potential conflict of interest.

Appendix A

Appendix A.1. Convergence Test

The purpose of the convergence study was to establish sufficiently stable Radiance sampling parameters for the matrix calculations. The BSDF representation was therefore held fixed during this assessment, while the relevant Radiance sampling parameters were progressively increased. Sensitivity to BSDF angular resolution is investigated separately in the main study through the systematic comparison of Klems and TT3–TT6 representations. The difference between two consecutive simulations is reduced when the ambient divisions increase. Only one convergence study was made in which the highest resolution of Shade_1A was used. The convergence study for the Three-Phase part of the Five-Phase Method is limited to Klems' resolution. The -aa, -ar, and -as were copied from the Reinhart reference office since the model in the study is based on the reference office; however, while these parameters were unchanged between all simulations, the crucial rcontrib parameters, -ad and -lw, were altered. Because the direct-sun component is particularly sensitive to sampling under conditions of high direct-light contribution, its convergence was assessed separately using point-in-time illuminance. The test was performed for the hour with the highest mean illuminance in the room (6 February at 12:00), providing a demanding condition for selection of the direct-sun sampling parameters. The convergence assessment

was performed using Shade_1A and was not repeated independently for each shading geometry. The selected parameters were subsequently held constant across all simulations so that BSDF resolution remained the controlled variable in the comparative analysis. The differences seem to be stabilising, and the chosen parameters are thus those used in simulation 7.

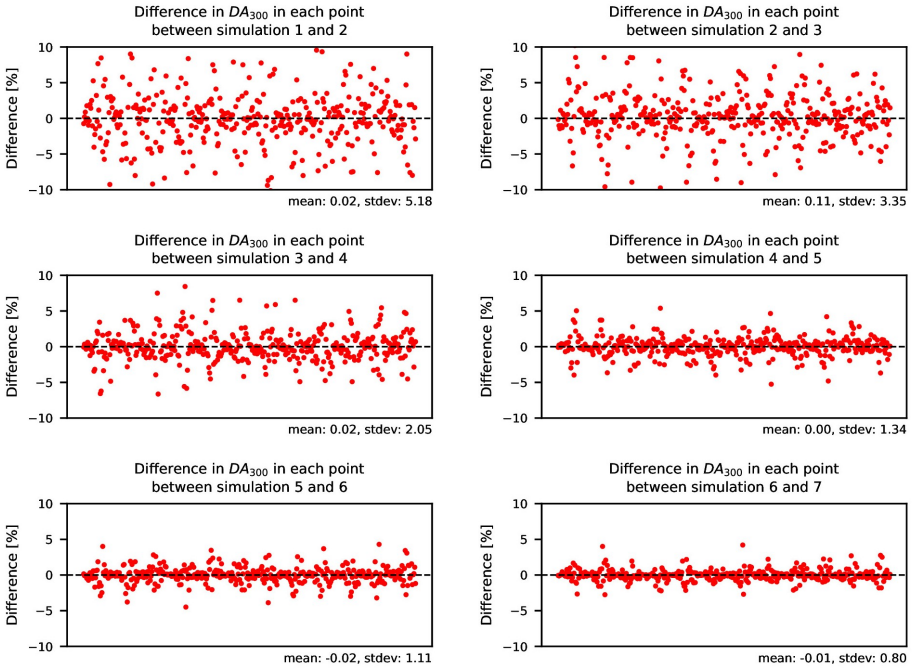


Figure A1. Difference in DA_{300} for each point between two consecutive simulations. The results are based on the simulations and parameters in Table 4.

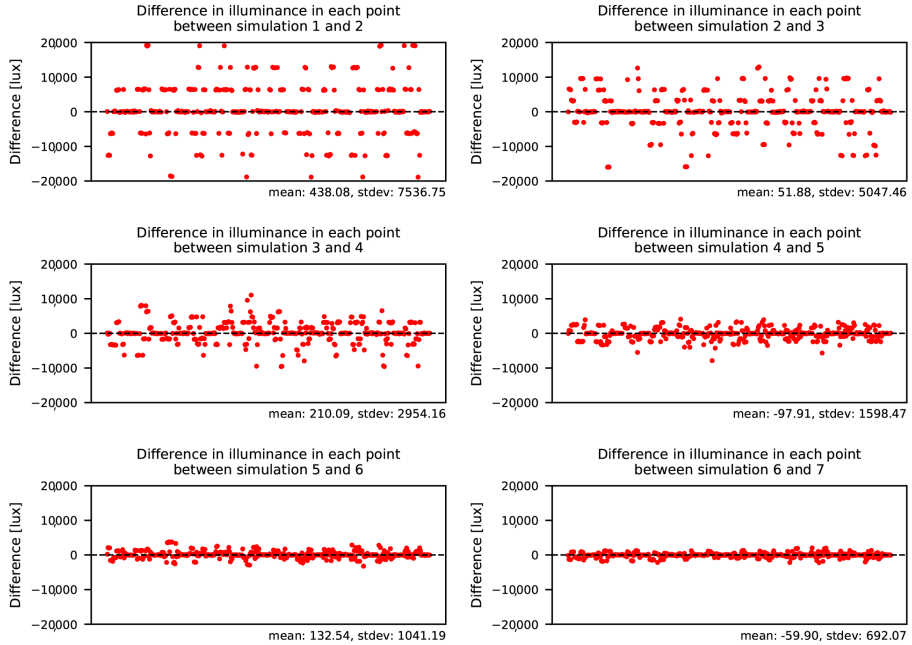


Figure A2. Difference in illuminance for each point between two consecutive simulations at February 6th 12:00. The results are based on the simulations and parameters in Table 6.

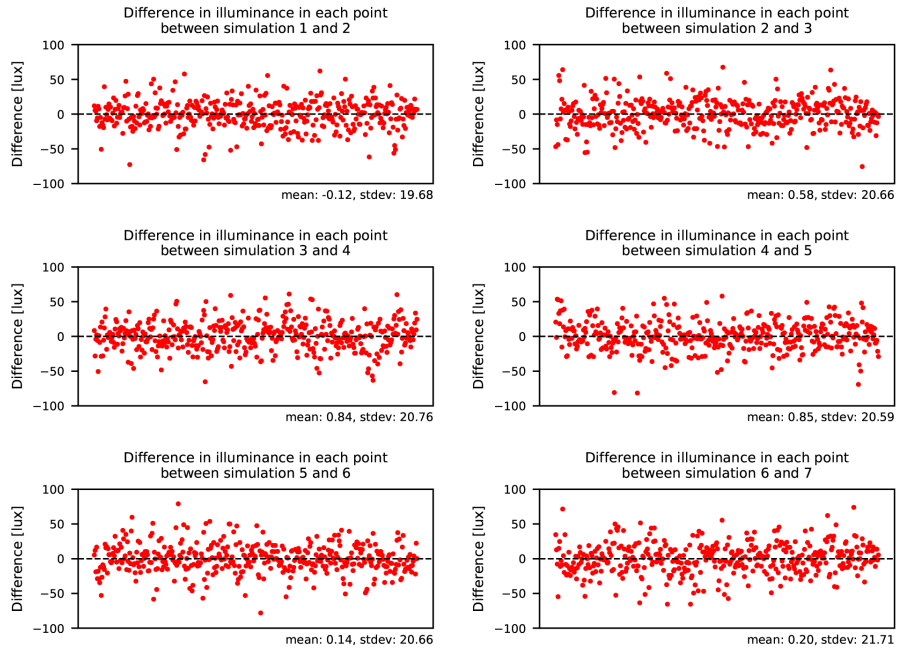


Figure A3. Difference in illuminance for each point between two consecutive simulations on March 21st at 12:00. The results are based on the simulations and parameters in Table 6.

Appendix A.2. Temporal Maps MAE

The Temporal Maps here show the MAE to TT6 resolution. Each map x-axis shows the different months of the year and the y-axis shows the time of the day. These graphs make it possible to identify the larger temporal errors areas for each shading system.

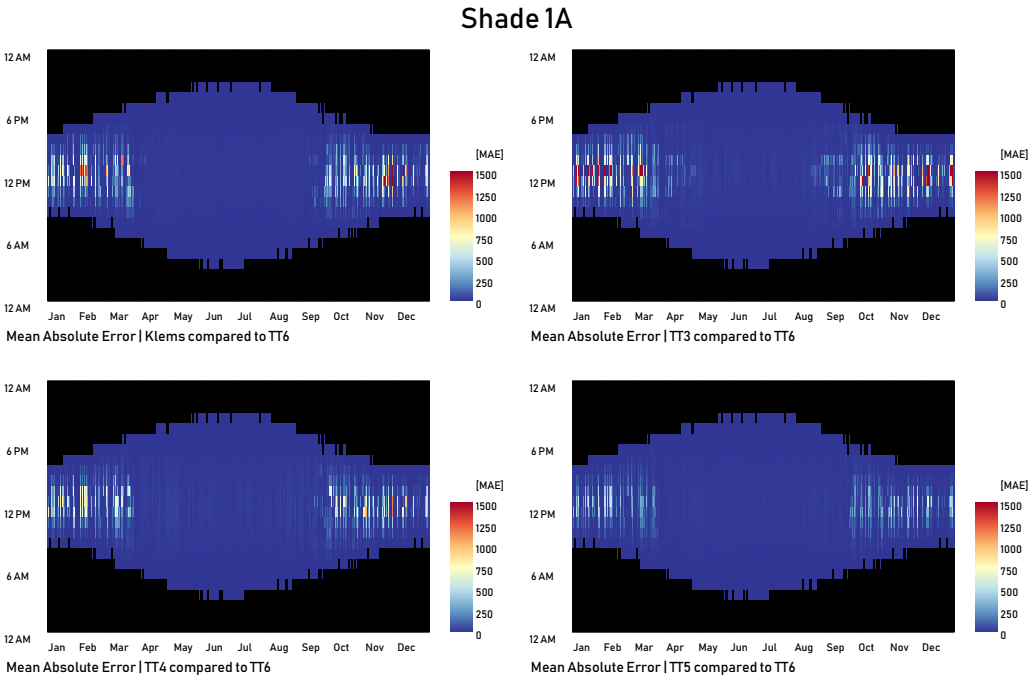


Figure A4. Annual MAE of illuminance for Shade 1A. The illuminance results of the BSDFs are compared to that of TT6.

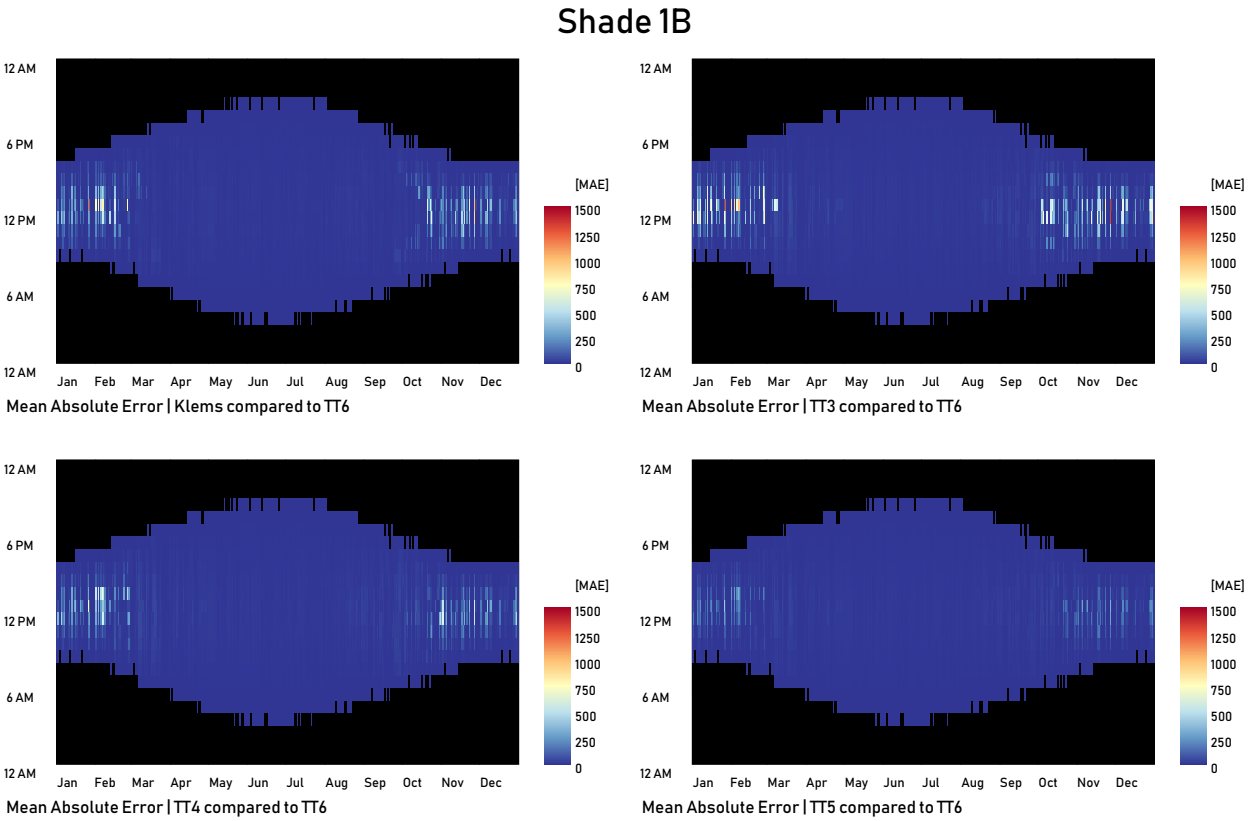


Figure A5. Annual MAE of illuminance for Shade 1B. The illuminance results of the BSDFs are compared to that of TT6.

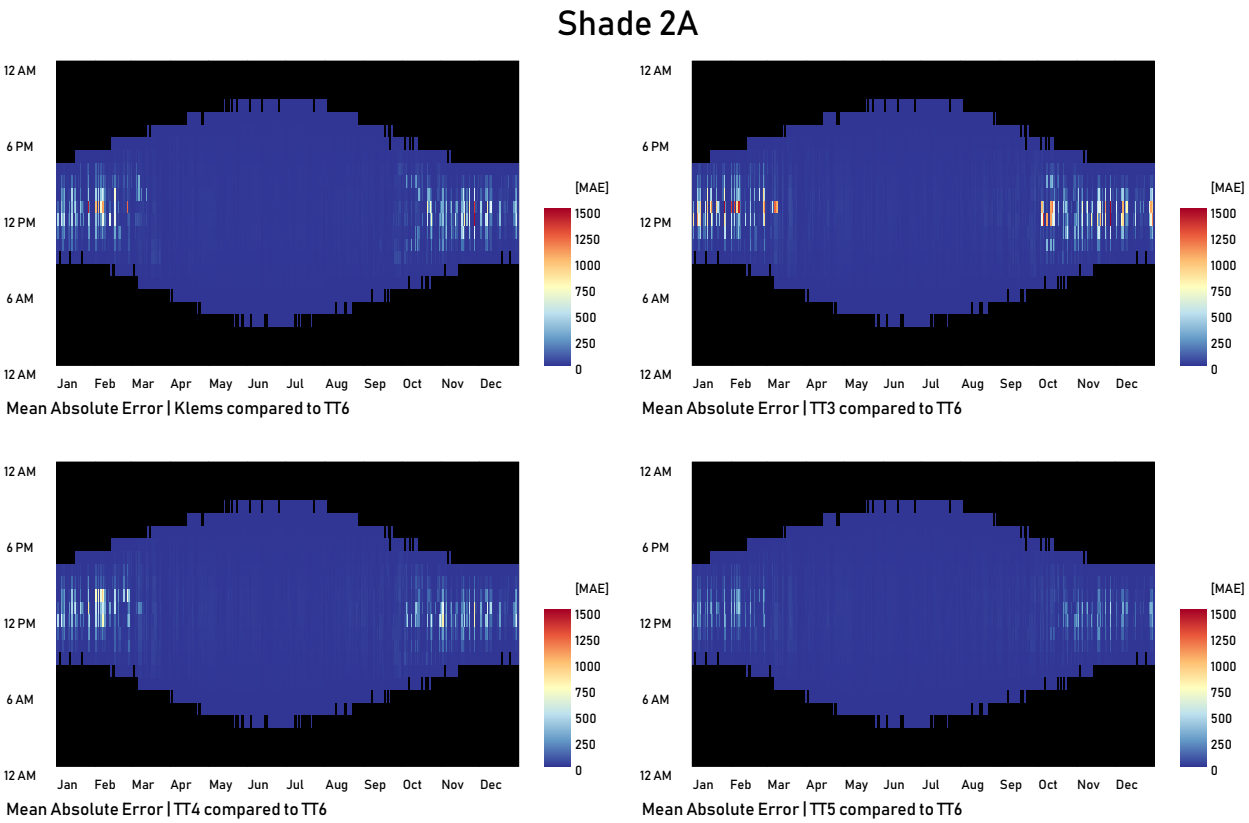


Figure A6. Annual MAE of illuminance for Shade 2A. The illuminance results of the BSDFs are compared to that of TT6.

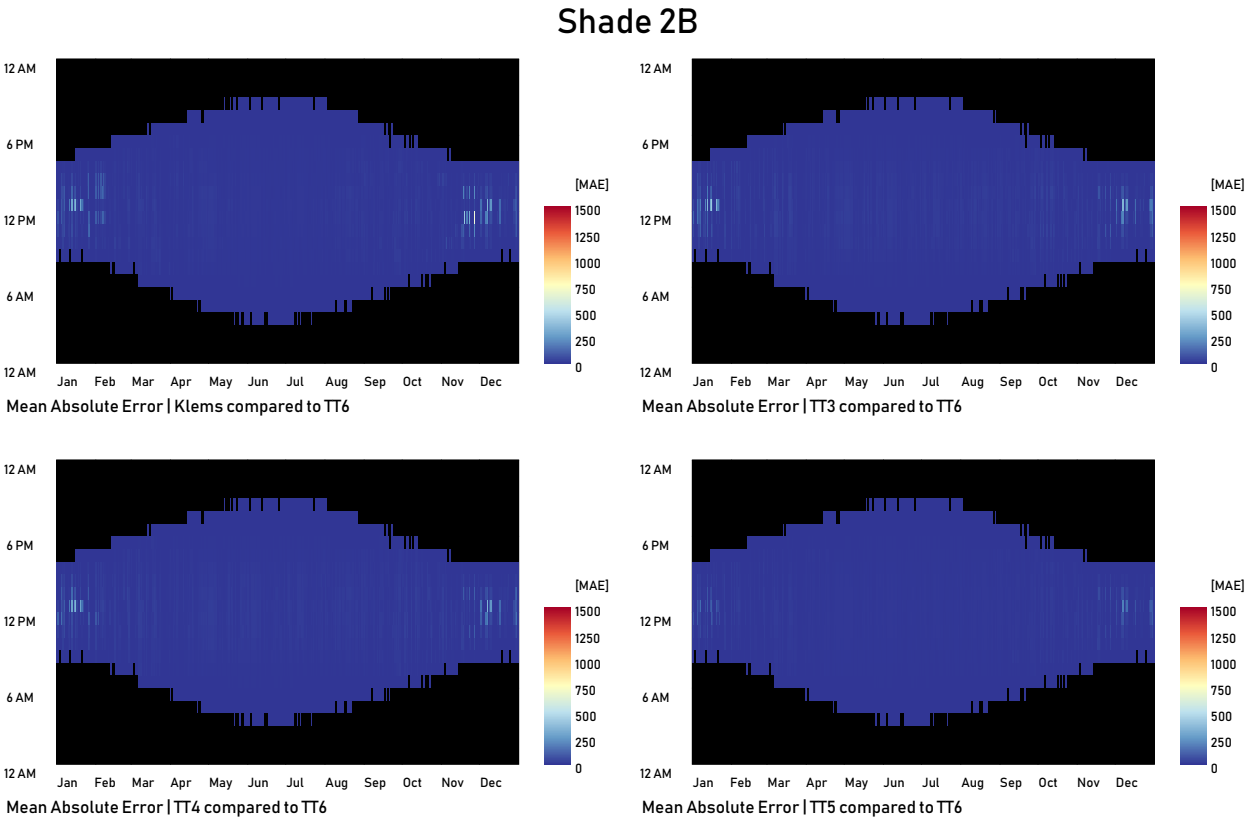


Figure A7. Annual MAE of illuminance for Shade 2B. The illuminance results of the BSDFs are compared to that of TT6.

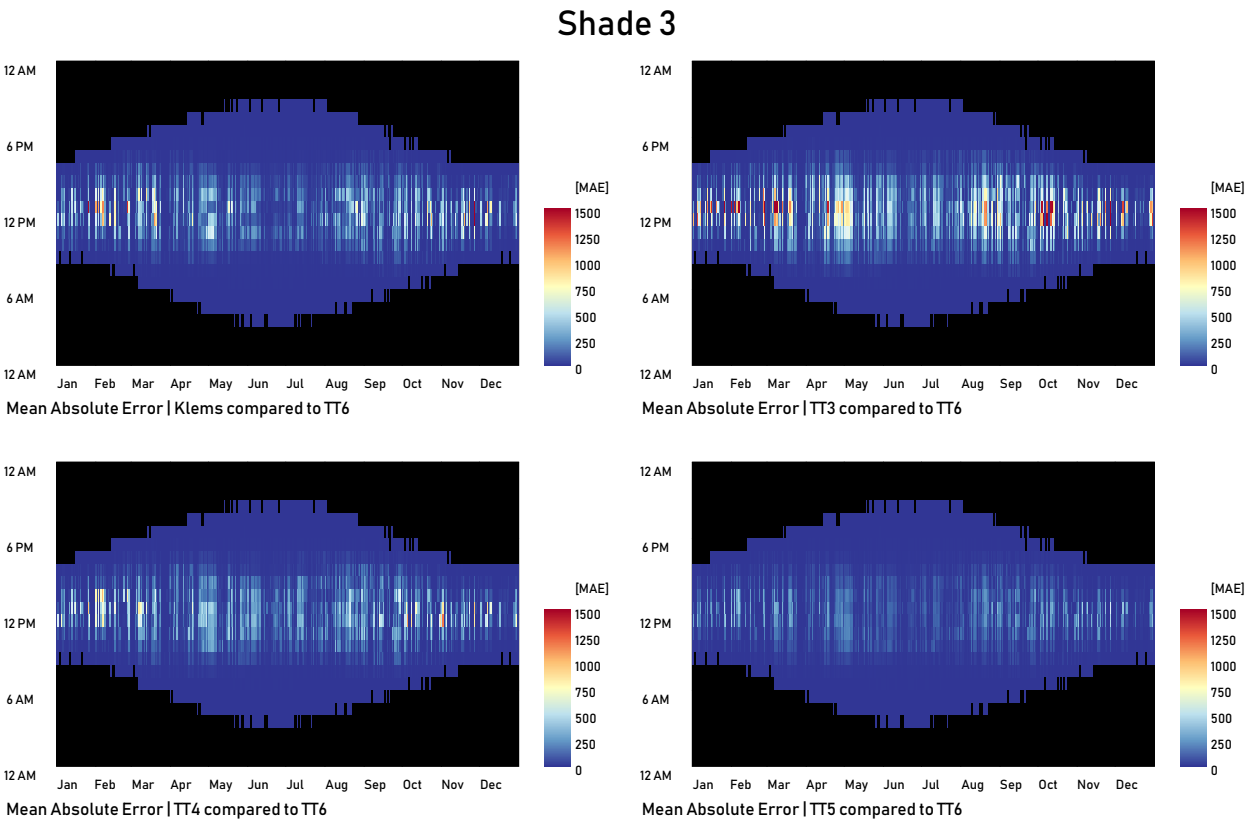


Figure A8. Annual MAE of illuminance for Shade 3. The illuminance results of the BSDFs are compared to that of TT6.

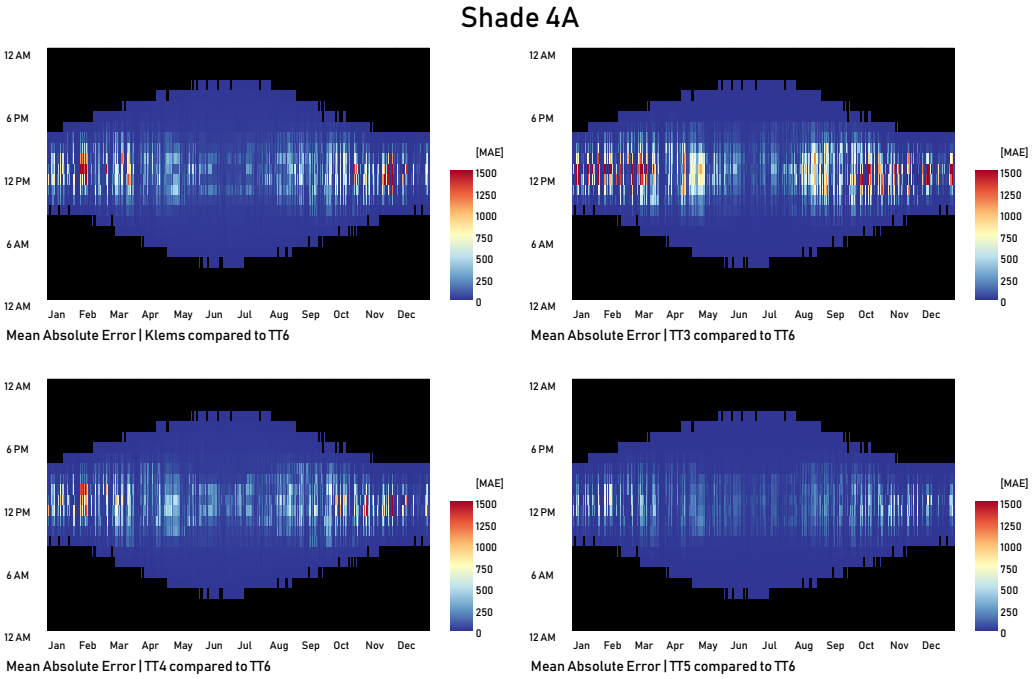


Figure A9. Annual MAE of illuminance for Shade 4A. The illuminance results of the BSDFs are compared to that of TT6.

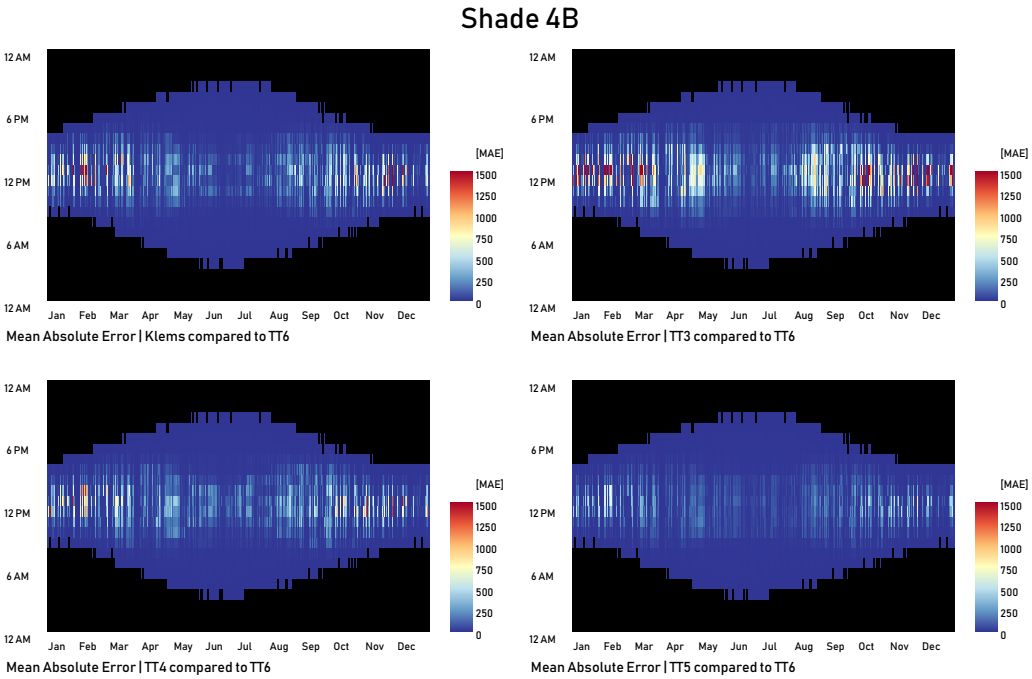


Figure A10. Annual MAE of illuminance for Shade 4B. The illuminance results of the BSDFs are compared to that of TT6.

References

1. Global Alliance for Buildings and Construction. *Global Status Report for Buildings and Construction Beyond foundations: Mainstreaming Sustainable Solutions to Cut Emissions from the Buildings Sector*; UNEP: Nairobi, Kenya, 2024. [CrossRef] [PubMed]
2. Intergovernmental Panel on Climate Change (IPCC). Buildings. In *Climate Change 2022: Mitigation of Climate Change. Working Group III Contribution to the Sixth Assessment Report of the Intergovernmental Panel on Climate Change*; Cambridge University Press: Cambridge, UK, 2023; pp. 953–1048. [CrossRef]

3. Ruck, N.; Aschehoug, O.; Aydinli, S.; Christoffersen, J.; Courret, G.; Edmonds, I.; Jakobiak, R.; Kischkoweit-Lopin, M.; Klinger, M.; Lee, E.S.; et al. *Daylight in Buildings: A Source Book on Daylighting Systems and Components*; IEA SHC Task 21/ECBCS Annex 29, Subtask A; Report No. LBNL-47493; LBNL: Berkeley, CA, USA, 2000. Available online: https://windows.lbl.gov/sites/default/files/daylight-in-buildings.pdf (accessed on 15 October 2026).
4. Bueno, B.; Wienold, J.; Katsifaraki, A.; Kuhn, T.E. Fener: A Radiance-based modelling approach to assess the thermal and daylighting performance of complex fenestration systems in office spaces. *Energy Build.* **2015**, *94*, 10–20. [CrossRef]
5. Khanie, M.S.; Andersen, R.K. Characterisation of view relative to solar-control systems. *Build. Environ.* **2024**, *265*, 112004. [CrossRef]
6. Tsangrassoulis, A. Shading and Daylight Systems. In *Energy Performance of Buildings: Energy Efficiency and Built Environment in Temperate Climates*; Boemi, S.-N., Irulegi, O., Santamouris, M., Eds.; Springer International Publishing: Cham, Switzerland, 2016; pp. 437–466. [CrossRef]
7. Kuhn, T.E. State of the art of advanced solar control devices for buildings. *Sol. Energy* **2017**, *154*, 112–133. [CrossRef]
8. McNeil, A.; Jonsson, C.J.; Appelfeld, D.; Ward, G.; Lee, E.S. A validation of a ray-tracing tool used to generate bi-directional scattering distribution functions for complex fenestration systems. *Sol. Energy* **2013**, *98*, 404–414. [CrossRef]
9. Ward Larson, G.; Shakespeare, R.A. *Rendering with Radiance: The Art and Science of Lighting Visualization*; Morgan Kaufmann Publishers: San Francisco, CA, USA, 1998.
10. Sacks, R.; Lee, G.; Burdi, L.; Bolpagni, M. *BIM Handbook: A Guide to Building Information Modeling for Owners, Designers, Engineers, Contractors, and Facility Managers*, 4th ed.; John Wiley & Sons: Hoboken, NJ, USA, 2025; 560p. [CrossRef]
11. Nicodemus, F.E.; Richmond, J.C.; Hsia, J.J.; Ginsberg, I.W.; Limperis, T. *Geometrical Considerations and Nomenclature for Reflectance*; NBS Monograph 160; National Bureau of Standards: Gaithersburg, MD, USA, 1977. [CrossRef]
12. Geisler-Moroder, D.; Lee, E.S.; Ward, G.; Bueno, B.; Grobe, L.O.; Wang, T.; Deroisy, B.; Wilson, H.R. *BSDF Generation Procedures for Daylighting Systems*; IEA SHC: Kingston, ON, Canada, 2021. [CrossRef]
13. Apian-Bennewitz, P.; de Boer, J.; Bueno, B.; Deroisy, B.; Fang, Y.; Geisler-Moroder, D.; Grobe, L.O.; Jonsson, J.C.; Lee, E.S.; Tian, Z.; et al. *Analysis and Evaluation of BSDF Characterization of Daylighting Systems*; IEA SHC: Kingston, ON, Canada, 2021. [CrossRef]
14. Klems, J.H. A New Method for Predicting the Solar Heat Gain of Complex Fenestration Systems: I. Overview and Derivation of the Matrix Layer Calculation. In Proceedings of the ASHRAE Winter Meeting, New Orleans, LA, USA, 22–26 January 1994; ASHRAE Transactions, Volume 100, Part 1.
15. CIE. *CIE Collection in Photometry and Radiometry. Technical Report CIE 114-1994*; Commission Internationale de l'Éclairage: Vienna, Austria, 1994; ISBN 978-3-900734-57-7.
16. Aydinli, S.; Kaase, H. *Measurement of Luminous Characteristics of Daylighting Materials: A Report of IEA SHC Task 21/ECBCS Annex 29*; International Energy Agency (IEA), Solar Heating and Cooling Programme: Paris, France, 1999. Available online: https://fils.iea-shc.org/Data/Sites/1/publications/report.pdf (accessed on 15 October 2026).
17. Ward, G.; Kurt, M.; Bonneel, N. Reducing Anisotropic BSDF Measurement to Common Practice. In Proceedings of the 2nd Eurographics Workshop on Material Appearance Modeling: Issues and Acquisition (MAM '14), Lyon, France, 25 June 2014; pp. 5–8. [CrossRef]
18. *ISO/CIE DIS 25176:2026*; Light and Lighting—Daylight in Buildings—BSDF Data Generation for Complex Fenestration Systems. International Organization for Standardization: Geneva, Switzerland, 2026; Draft International Standard (Under Development). Available online: https://www.iso.org/standard/89258.html (accessed on 15 October 2026).
19. Geisler-Moroder, D.; Lee, E.S.; Apian-Bennewitz, P.; de Boer, J.; Bueno, B.; Deroisy, B.; Fang, Y.; Grobe, L.O.; Hauer, M.; Hoffmann, S.; et al. BSDF Data Generation for Daylight Applications: A Call for International Standardization. *Light. Res. Technol.* **2025**, *57*, 579–603. [CrossRef]
20. Ward, G.; Mistrick, R.; Lee, E.S.; McNeil, A.; Jonsson, J.C. Simulating the Daylight Performance of Complex Fenestration Systems Using Bidirectional Scattering Distribution Functions within Radiance. *LEUKOS* **2011**, *7*, 241–261. [CrossRef]
21. McNeil, A.; Lee, E. A validation of the Radiance three-phase simulation method for modelling annual daylight performance of optically complex fenestration systems. *J. Build. Perform. Simul.* **2013**, *6*, 24–37. [CrossRef]
22. Lee, E.S.; Geisler-Moroder, D.; Ward, G. Modeling the direct sun component in buildings using matrix algebraic approaches: Methods and validation. *Sol. Energy* **2018**, *160*, 380–395. [CrossRef]
23. Grobe, L.O. Photon mapping in image-based visual comfort assessments with BSDF models of high resolution. *J. Build. Perform. Simul.* **2019**, *12*, 745–758. [CrossRef]
24. Ward, G.J.; Wang, T.; Geisler-Moroder, D.; Lee, E.S.; Grobe, L.O.; Wienold, J.; Jonsson, J.C. Modeling specular transmission of complex fenestration systems with data-driven BSDFs. *Build. Environ.* **2021**, *196*, 107774. [CrossRef]
25. Geisler-Moroder, D. BSDF Daylight System Characterization—Sensitivity and Requirements to Resolution. In Proceedings of the 18th International Radiance Workshop, New York, NY, USA, 21–23 August 2019.
26. Kischkoweit-Lopin, M. An overview of daylighting systems. *Sol. Energy* **2002**, *73*, 77–82. [CrossRef]

27. Mainini, A.G.; Poli, T.; Zinzi, M.; Speroni, A. Spectral light transmission measure of metal screens for glass facades and assessment of their shading potential. *Energy Procedia* **2014**, *48*, 1292–1301. [CrossRef]
28. Andersen, M.; Rubin, M.; Powles, R.; Scartezzini, J.L. Bi-directional transmission properties of Venetian blinds: Experimental assessment compared to ray-tracing calculations. *Sol. Energy* **2005**, *78*, 187–198. [CrossRef]
29. Ibrahim, A.; Alsukkar, M.; Eltaweel, A.; Hermaputi, R.L. Multi-Objective Optimization of Daylighting for an Office Space in a Very Hot Climate: A Comparison of Corrugated, Perforated, and Separated Shadings. *Buildings* **2026**, *16*, 2625. [CrossRef]
30. Ibrahim, A.; Alsukkar, M.; Wang, L.; Hermaputi, R.L.; Dong, Y.; Yin, S.; Xiao, Y.; Hu, P. Targeting integrated daylighting comfort in deep office by multi-objective optimization using partial vertical deployment of adaptive corrugated shadings. *Energy Built Environ.* **2026**. [CrossRef]
31. Reinhart, C.; Jakubiec, J.; Ibarra, D. Definition of a reference office for standardized evaluations of dynamic facade and lighting technologies. In Proceedings of the 13th Conference of IBPSA, Chambéry, France, 25–28 August 2013. [CrossRef]
32. Subramaniam, S. *Daylighting Simulations with Radiance Using Matrix-Based Methods*; Technical Report/Tutorial; Lawrence Berkeley National Laboratory (LBNL): Berkeley, CA, USA, 2017. Available online: https://www.radiance-online.org/learning/tutorials/matrix-based-methods (accessed on 15 October 2026).
33. Molina, G.; Bustamante, W.; Rao, J.; Fazio, P.; Vera, S. Evaluation of radiance's genBSDF capability to assess solar bidirectional properties of complex fenestration systems. *J. Build. Perform. Simul.* **2015**, *8*, 216–225. [CrossRef]
34. Haghani, M.; Jonsson, J.C.; Salamati, M.; Place, W. Comparative assessment of optical characterization of prismatic materials (PMs), using genBSDF tool for virtual simulations and a goniophotometer for physical measurements. *Build. Environ.* **2023**, *238*, 110323. [CrossRef]
35. *EN 17037:2018+A1:2021*; Daylight in Buildings. European Committee for Standardization (CEN): Brussels, Belgium, 2021.
36. Wang, T.; Lee, E.S.; Ward, G.J.; Yu, T. Field validation of data-driven BSDF and peak extraction models for light-scattering fabric shades. *Energy Build.* **2022**, *262*, 112002. [CrossRef]

Disclaimer/Publisher's Note: The statements, opinions and data contained in all publications are solely those of the individual author(s) and contributor(s) and not of MDPI and/or the editor(s). MDPI and/or the editor(s) disclaim responsibility for any injury to people or property resulting from any ideas, methods, instructions or products referred to in the content.